

Sarah E. Gasda, Elsa du Plessis, and Helge K. Dahle

Upscaled models for CO₂ injection and migration in geological systems

Abstract: Geological sequestration of CO₂ may be an important tool to reduce anthropogenic emissions of greenhouse gases. To predict the long-term fate of the CO₂ plume and ultimately reduce the risks involved in injecting vast amounts of supercritical CO₂ into underground formations, simulation studies are necessary. However, because of large temporal and spatial variations in scale, realistic scenarios based on modeling can only be achieved through semi-analytical or upscaling techniques.

In this chapter, we review progress and limitation of upscaling methods based on assuming vertical equilibrium in the two-phase flow system. Using dimensional groupings, we show that these formulations are adequate for conditions that will occur in many typical storage scenarios. We then review the inclusion of capillarity, dissolution, compressibility, and caprock topography into these models. We review some of the benchmarking that has been performed on these types of methods, and finally give some simulation results based on realistic storage conditions.

Keywords: Geological CO₂ Sequestration, Vertical Equilibrium, Capillary Fringe, Dissolution, Convective Mixing, Compressibility, Caprock Rugosity, Benchmarking, Upscaled Model, Dimensionless Group.

Mathematics Subject Classifications 2010: 76S05, 35Q35

Sarah E. Gasda: Uni CIPR, Bergen, Norway, sarah.gasda@uni.no

Elsa du Plessis: Department of Mathematics, University of Bergen, Bergen, Norway,
elsa.plessis@math.uib.no

Helge K. Dahle: Department of Mathematics, University of Bergen, Bergen, Norway,
helge.dahle@math.uib.no

1 Introduction

Storage of carbon dioxide (CO₂) in deep geological formations has been proposed as a viable technology to mitigate greenhouse gas emissions [7, 44]. In order for geological CO₂ storage to be successful, large volumes of CO₂ on the order of a billion metric

This work was supported in part by the MatMoRA project (Mathematical Modelling and Risk Assessment of CO₂ storage), Contract no. 215641, and the VAMP project (Development and Analysis of Vertically Averaged Models in Porous Media), Contract no. 199926, financed by the CLIMIT program of the Research Council of Norway and Statoil. The authors would also like to thank H. Nilsen and O. Andersen at SINTEF ICT and the anonymous reviewers for providing thoughtful comments.

tons annually must be stored reliably and efficiently for 1000 years or more [56]. Detailed modeling and numerical simulations will be required to evaluate the feasibility of potential sequestration sites, in particular models will be needed to predict the ultimate fate of the CO₂ plume and assess possible risks associated with the large-scale migration over long timescales [50].

In prospective sites for CO₂ storage, such as a saline aquifer or abandoned petroleum reservoir, the subsurface conditions are such that CO₂ is a supercritical fluid [4] and slightly soluble in water (the solubility limit is about 4% by volume [19]) and thus forms a separate fluid phase that is less dense and much less viscous than the resident brine [51]. This results in a two-phase flow system in which the injected CO₂ will spread radially away from the injection well and displace the brine, whereas buoyancy forces will cause CO₂ to move progressively higher in the formation. The upward movement of the CO₂ plume will typically be constrained by a low-permeability caprock that bounds the aquifer above.

Accurate and efficient models are required that can resolve the two-phase flow physics within very large spatial and temporal domains associated with CO₂ storage. In addition, other relevant aspects of CO₂ migration and trapping need to be captured. For instance, the migration of CO₂ can be affected by local capillary effects [53], the rock can deform due to thermomechanical stresses [59, 66], and CO₂ dissolution in brine can be enhanced by density-driven convection under the plume fringe [20]. Other salient processes include the creation of “wet” CO₂ due to evaporation of water into the CO₂-phase, a drying front behind the CO₂ injection front that corresponds to dry CO₂ in the formation [49], and salt precipitation [62], among others. This full suite of physical processes must be modeled given the heterogeneity and structural complexity typical of most sedimentary systems.

Numerous state-of-the-art modeling frameworks have been applied to CO₂ injection and storage in geological systems ([68] and references therein). Multipurpose numerical simulators for multiphase flow and transport in porous media, e.g. TOUGH2 [63] and ECLIPSE [67], allow for injection of CO₂ and modeling of heat and chemical species transport in heterogeneous three-dimensional geological systems. However, a significant challenge faced by traditional numerical approaches is the ability to resolve the relevant physics described above. This has been demonstrated in recent benchmark studies (e.g. [10]), where the task of providing spatially resolved, “full-physics” solutions in 3D proved to be inherently difficult. Part of the challenge is that gravity override leads to a very thin CO₂ fringe under the caprock, and resolving this fringe requires high vertical grid resolution; in particular, caprock topography, or roughness, have a strong impact on the distribution and areal extent of the CO₂ plume [28]. Likewise, the dynamics entails inherently unstable phenomena like convective dissolution [40, 57, 65] that necessitate highly resolved grids in the horizontal direction. The resolution requirements of these types of coupled systems are thus computationally intractable in large-scale CO₂-storage systems.

These computational challenges have led to the reemergence of upscaled models that resolve the physical processes in an average sense based upon depth integration. In this chapter, we present a review of recent advances in vertically integrated models and their application to CO₂ storage systems. We discuss the fundamental assumptions inherent in the vertically integrated approach and identify the range of validity of the model using several dimensionless groupings. The vertical equilibrium (VE) model equations are then formulated for the incompressible, immiscible case that accounts for non-linearities associated with capillary effects. The model is extended to account for subscale processes that may significantly impact CO₂ migration and trapping, including CO₂ compressibility, dissolution with convective mixing and subscale caprock roughness. Finally, several applications of the vertically integrated model are presented that show the practical benefits of the simplified modeling approach for real CO₂ storage systems.

2 Background

Large-scale and long-term storage of CO₂ in subsurface aquifers, as represented in Figure 1.1, presents a complex challenge in which multiple processes take place across various spatial and temporal scales. Including all of these processes over all relevant scales in a simulation to predict the long-term fate of the injected CO₂ leads to many complications, the result of which may not necessarily be an accurate prediction due to the inherit complexity of the entire system [49]. It is thus important to consider

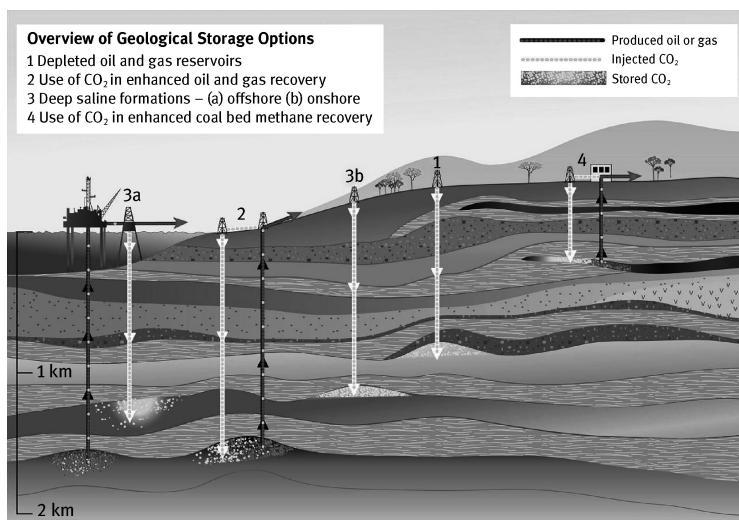


Figure 1.1: Storage of CO₂ in deep subsurface formations. Figure adapted from the IPCC report on carbon dioxide capture and storage [44].

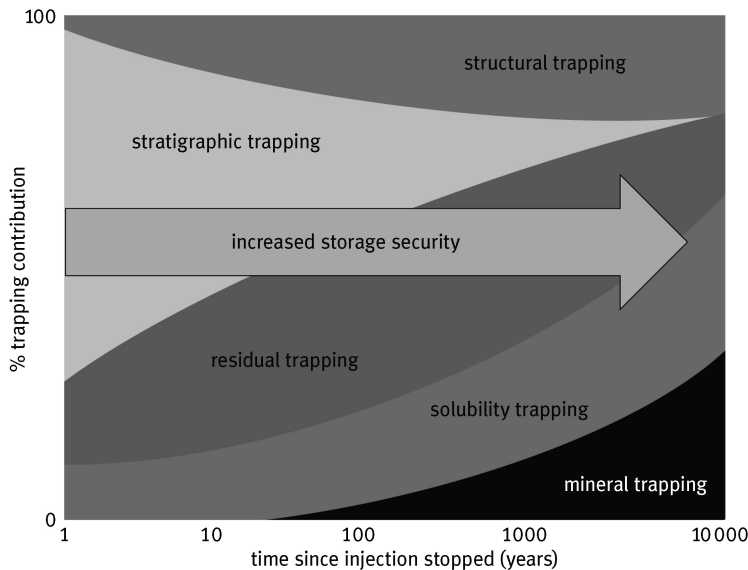


Figure 1.2: Schematic with the range of considered temporal scales with regards to increasing storage security in a CO₂-injection model. Figure adapted from the IPCC report on carbon dioxide capture and storage [44].

at which scales particular processes are dominant, and further, which processes are of most importance and which could possibly be considered negligible to simplify the modeling process.

Considerations across the spatial scales range from the interactions between CO₂ and brine at the pore scale, to the eventual lateral extent of both the CO₂ and pressure plumes on the aquifer scale. Similarly, temporal scale considerations range from the establishment of capillary equilibrium over a relatively brief timescale to the 1000-year timescale after which CO₂ is considered to be safely stored according to proposed guidelines [50]. Between both the extreme length and timescales are a multitude of other complex processes that may dominate over intermediate scales, which could in turn greatly affect plume-migration predictions.

Possible processes and model parameters affecting storage security across various timescales are represented in Figure 1.2. Immediately after injection, CO₂ is confined to the storage aquifer solely by stratigraphic or hydrodynamic trapping, e.g. a relatively impermeable caprock. As time progresses postinjection, residual trapping of CO₂, occurring on the pore scale, traps an increasing portion of CO₂ mass along with other interfacial behavior such as equilibrium partitioning. Over longer timescales, dissolution due to convective mixing [16] driven by centimeter-scale instabilities may act to enhance solubility trapping [16, 50]. Larger spatial scale considerations include the caprock topography [25], which could vary on the order of cen-

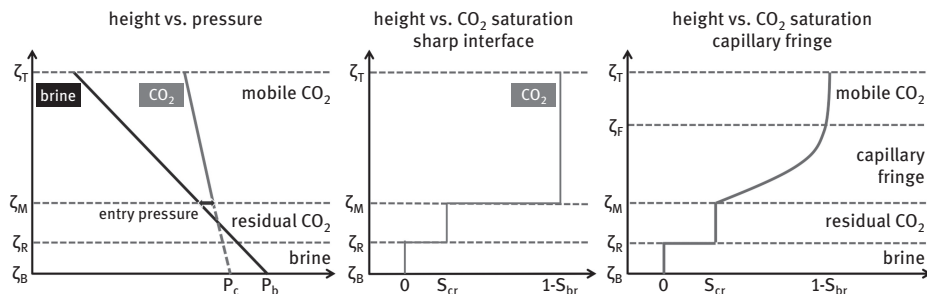


Figure 1.3: Pressure profiles of brine and CO₂ across the height of the aquifer under the VE assumption. Two different CO₂ saturation profiles correspond to the pressure profile (left) – a sharp interface assumption with abrupt saturation change at ζ_M (middle) and a capillary transition zone that leads to gradual saturation within the two-phase fringe (right).

timeters to meters yet may impact CO₂ migration over hundreds of kilometers. Such a phenomenon would lead to an increased amount of trapped of CO₂ at later times due to this structural heterogeneity. Mineral reactions that lead to mineral trapping occurs at the very lower end of the spatial spectrum and becomes increasingly important with regards to storage security at the far end of the temporal scale [50]. These slow reactions are separate from fast mineral reactions that may impact flow patterns near the injection well or enhance leakage along an old abandoned well.

The approach of using upscaling methods to simplify modeling of these large systems stems from taking advantage of the length scales relevant in geological systems which are deemed suitable for long-term storage of CO₂ [50]. Suitable sites under consideration for CO₂ injection are generally characterized by aquifers with a much greater horizontal span compared to the vertical. The proposed method is to reduce the dimensionality of the problem by upscaling the model parameters across the vertical span and to advance the solution across the horizontal extent of the aquifer, thus greatly reducing the computational cost.

Historically, it is exactly this computational cost of a full three-dimensional simulation that drove the development of upscaled models for fluid flow in reservoir simulations. Martin [43] proposed a mathematical framework whereby the equations for multiphase, three-dimensional compressible flow were reduced to a set of two-dimensional equations for the fluid flow in a reservoir through vertical integration of the model parameters. Importantly, the effects of fluid segregation due to density differences, as well as the effects of capillarity, which are both present across the vertical scale of a reservoir, were included in the simplified model. Martin's [43] framework built on and verified the work of Coats [11], in which the concept of VE was first introduced in reservoir engineering.

The crucial assumption of VE refers to a multiphase system in which the establishment of a pressure equilibrium across the vertical dimension occurs much faster

than the advancement of the actual saturation plume. The VE assumption translates into a system with negligible vertical flow and a hydrostatic pressure distribution of each phase, where gravitational and capillary forces are in equilibrium. Figure 1.3 represents the pressure profiles under the VE condition across the vertical extent of the aquifer of the resident brine and the injected CO₂, with quantities on the vertical axis denoting the respective interfaces in the system between the top and bottom of the aquifer. The pressure change in each phase is constant across the aquifer height which in turn implies that the change in capillary pressure is also constant across the aquifer height.

Given VE conditions, the upscaling techniques to obtain a mathematical VE model have historically started from the macroscale multiphase flow theory, including Darcy's law and local constitutive functions, i.e. relative permeability and capillary pressure relations. These three-dimensional equations are subsequently upscaled by integrating across the storage formation thickness. Alternative approaches have been suggested, such as the method developed by Gray et al. [29] which proposes direct integration from the microscale to the vertically integrated scale, a more complete derivation and one that can be constrained by thermodynamic relations of the system. This derivation has been applied previously to CO₂ storage systems [28].

The historical work of Martin [43] and Coats [11] came at a time when computational capabilities were very limited, making full scale reservoir simulation in especially the petroleum engineering industry [12, 14, 38] particularly challenging. Since then computational power and numerical methods have progressed significantly, yet the method of upscaling and the assumption of VE is still relevant and useful today. Such models are quite common in physics [33] but have enjoyed renewed interest in recent years with application to CO₂ injection into saline aquifers [30, 31, 37, 54]. Simplified models have recently been used in combination with Monte Carlo techniques [49, 51, 52] to assess leakage risks when a CO₂ plume contacts thousands of abandoned wells, a task that would be impossible to perform using standard simulation techniques. Likewise, analytical solutions for CO₂ gravity currents have been developed [31–33, 37, 42] to enable simplified calculations of the CO₂ inventory (free-phase CO₂, residual trapped CO₂, and possibly dissolved CO₂).

The reliability of these simplified models has been tested in a recent benchmark study [10], where an application of a VE model [22] to the Johansen formation produced qualitatively comparable results to those obtained by commercial codes resolving the full three-dimensional problem. A study on the application of a VE model to the Utsira formation [48] revealed that the simplified model could deliver more accurate results when full fluid segregation had taken place compared with a fully three-dimensional ECLIPSE simulation. In addition, the VE simulation proved to be significantly faster, and have thus proved to be an effective means to test different model choices and explore parameter spaces.

Vertical equilibrium models certainly have restrictions in their applicability and as such should not be expected to provide accurate results through all phases of CO₂

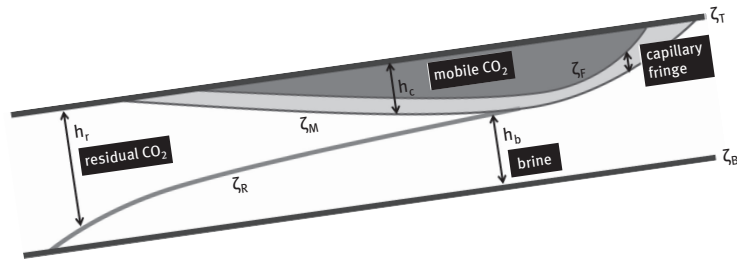


Figure 1.4: Sharp interface model with heights of brine, mobile CO₂, and residually trapped CO₂.

injection and storage [41]. As previously discussed, these models were developed for segregated fluids. In modeling the spread of a CO₂ plume, it should thus be noted that vertical fluid segregation due to the density difference of brine and supercritical CO₂ may not occur immediately and uniformly across the plume. The influence on vertical flow in highly anisotropic geological systems should also be considered, as these effects would not necessarily be captured by a simplified VE model. Various dimensionless groupings, discussed in more detail later, allow the specific system and spatial/temporal scales of interest to be analyzed and determine whether the fundamental assumptions of equilibrium are valid. In general, the VE model formulation is often better suited for predicting the long-term migration of injected CO₂ in reasonably heterogeneous aquifers where buoyancy effects are strong and the aspect ratio is high. Application during the injection phase is also suitable if the viscous-dominated region near the injection well is small and/or the near-well flow dynamics are not of primary interest.

Current VE models have been developed through integration of governing equations written at the Darcy scale (macro scale) and upscaled to the aquifer scale [50]. It is at this scale where results pertaining to the migration of the CO₂ plume are of interest. At the macroscale the equations for multiphase flow are written in terms of the respective saturations. The large aspect ratio of the aquifer may then be exploited in upscaling of the macroscale model, where the saturations are modeled as heights of the layers of each phase as in Figure 1.4. In this model it has been assumed that the interfaces between the phases are sharp [50]. The CO₂ plume is traveling up-slope above the resident brine in this formation, leaving a trail of residually trapped CO₂ in its wake. The simplicity of this model greatly reduces computational cost, and yet, as demonstrated by Nilsen et al. [48], delivers quantitatively accurate results when compared with commercial codes that resolve the fully three-dimensional scenario.

A simplified model such as the one depicted in Figure 1.4 could be extended to include more complex behavior in the system, depending on the primary goal of the simulation. It is possible to include effects of dynamic processes on the microscale by keeping track of changes in all three dimensions and upscaling again [50]. Through such a method there is continuous multiscale communication, ensuring that

any significant changes on the finer scale influence the upscaled model appropriately. Fine scale processes that could impact the eventual plume migration include relative permeabilities, the formation of a capillary fringe [53] and hysteretic effects.

The basic VE model starts off assuming a two-phase, immiscible system with a sharp interface and a regular, heterogeneous aquifer. Recent developments in increasing the complexity of this model include modeling the capillary fringe [53] and different trapping mechanisms within the system. Structural trapping, whereby pockets of CO₂ could potentially be immobilized and trapped between irregularities at the caprock interface, has been shown to be significant [25, 48]. In addition, Mykkeltvedt and Nordbotten [45] have studied the effects of convective mixing on the plume migration.

The development of simulators that implement the VE model is part of ongoing work. Because the simplified 2D model equations are analogous to the full three-dimensional system but with different definitions of the coarse-scale variables and constitutive functions, many of the same numerical methods can be applied to the VE model. Further developments have been made regarding the computational implementation of VE models, with the open-source MATLAB Reservoir Simulation Toolbox (MRST), developed by Nilsen et al. [48] available as an alternative to existing commercial codes [69]. The key focus in numerical implementation is on increasing efficiency. Although a key factor in efficiency is having fewer equations in a reduced dimension system, the VE model also weakens the pressure-transport coupling and eliminates the timestep restrictions that result from vertical resolution of sharp fronts required in 3D codes [34].

3 Model description

We describe the development of a simplified model for CO₂ injection, migration and trapping into a storage formation. The storage formation, which is defined as either the thickness of an entire permeable formation or of one stratified layer created by vertical heterogeneity in the formation, is initially saturated with brine and is bounded above and below by relatively impermeable shale formations. As depicted in Figure 1.4, the top and bottom boundaries are described by depth surfaces $\zeta_T = \zeta_T(x, y)$ and $\zeta_B = \zeta_B(x, y)$, respectively. In general, the storage formation may be heterogeneous with respect to geometry and other geological parameters.

We consider CO₂ injection into the storage formation as a two-phase two-component system. The CO₂-rich phase is denoted by subscript *c* whereas the brine-rich phase is denoted by subscript *b*. CO₂ migration is driven predominantly by gravity and viscous forces. CO₂ trapping occurs by three predominant mechanisms – structural trapping in local traps and domes, residual trapping due to capillary snap-off during imbibition, and solubility trapping due to CO₂ dissolution into the resi-

dent brine. We do not consider mineralization trapping, which occurs on a longer timescale than of interest.

The key aspects of the model development are integration over the vertical dimension of the storage formation and the simplifying assumptions associated with this upscaling procedure. Vertical integration is an upscaling step that coarsens the fine-scale model from three dimensions to two lateral dimensions. Thus, the “fine-scale” is defined as the full three-dimensional model that resolves the vertical dimension, while the “coarse-scale” is a two-dimensional model that represents the fine-scale vertical distribution with coarse-scale or average variables. We note that the horizontal scale of the fine- and coarse-scale models may be the same. Simplifying assumptions are needed to define coarse-scale variables as a function of fine-scale quantities and to reconstruct the solution at the fine scale if desired.

The simplified model derivation from three-dimensional REV-scale equations is described in this section. However in previous work, the VE model has been derived from the microscale directly to the depth-integrated scale [28]. To begin, we will summarize the conceptual framework as well as identify and describe the assumptions employed in the coarse-scale model development. These assumptions are not necessary for integration of the three-dimensional equations and may be relaxed depending on the system of interest.

3.1 Key assumptions and dimensionless groupings

The key assumptions for application of the VE model are as follows:

- large aspect ratio of the storage system;
- strong buoyancy effects;
- capillary–gravity equilibrium; and
- aquifer with modest heterogeneity and dip angle.

The necessary attributes of the storage system will be explored further here.

The first element of vertical integration is the assumption of VE at the fine scale. VE implies that pressure is in fluid-static equilibrium and vertical flow can be neglected. Fundamentally, VE requires a system with a large aspect ratio, i.e. the horizontal length scale (L) is significantly greater than the vertical (H) [70]. To determine the validity of VE for a given system, a dimensionless grouping can be formed using the aspect ratio and the permeability anisotropy ratio k_H/k_V

$$R_L^{-1} = \frac{H}{L} \sqrt{\frac{k_H}{k_V}}. \quad (1.1)$$

VE is a valid assumption when $R_L \gg 1$.

The VE assumption for a system with two fluids of different density implies fluid segregation due to gravity within a relatively short time. A dimensionless timescale

for gravity segregation can be formulated [53] as

$$T_v = T \frac{\lambda_c^* k_V \Delta \rho g \cos \theta}{\phi H}, \quad (1.2)$$

which consists of the density contrast between the two fluids $\Delta \rho = \rho_b - \rho_c$, gravitational constant g , endpoint CO₂ mobility at residual brine saturation λ_c^* , characteristic time T of the modeled system, vertical permeability k_V , porosity ϕ , formation dip angle θ and formation thickness H . We may assume complete gravity segregation within the timescale of interest when $T_v \gg 1$. There may be regions of the system where $T_v \ll 1$ due to strong viscous forces, e.g. close to the injection well. However, if vertical segregation has occurred over the majority of the plume, then the VE model may be applied during injection. When near-well dynamics are of primary interest then either a 3D model or some other upscaling/coupling techniques are required.

In addition to gravity forces, we must also consider capillary forces that act to disperse the two fluid phases over some characteristic length scale. Contrary to gravity, which forces the lighter fluid to be on top of the denser fluid, local capillarity disperses the lighter fluid downward and forms a transition zone, or capillary fringe, within which both fluids exist and are mobile. At equilibrium, the capillary and gravity forces are balanced, and the local distribution of saturation within the capillary fringe are fixed according to the local capillary-pressure saturation curve. The fringe has a dimensionless length scale ϵ [53],

$$\epsilon = \frac{p_c^*}{\Delta \rho g \cos \theta H}, \quad (1.3)$$

where p_c^* is the characteristic capillary pressure from the local p_c function for a given system. When $\epsilon \ll 1$ the fringe is relatively small and can be neglected, while when $\epsilon \gg 1$, then the transition zone is large and should be captured by the upscaled model.

The timescale to establish a capillary fringe (at capillary–gravity equilibrium) can be described by the dimensionless time [53],

$$T_f = T \frac{k_V}{\phi} \frac{\lambda_c^* \lambda_b^* p_c^*}{(\lambda_c^* + \lambda_b^*)(\epsilon H)^2}. \quad (1.4)$$

This timescale of vertical movement may be compared to the timescale associated with horizontal flow T_h ,

$$T_h = T \frac{\lambda_c^* k_H \Delta \rho g \sin \theta}{H \phi (1 - s_{br})} \quad (1.5)$$

with the residual brine saturation denoted as s_{br} . We may assume a capillary fringe has been established when the $T_f \gg 1$ and $T_h/T_f \ll 1$.

The final aspect is related to variation in caprock topography below some prescribed scale of the model resolution. The caprock roughness acts to retard CO₂ migration and increase subscale structural trapping. The strength of caprock roughness

factor decreases as the capillary fringe thickness increases. A dimensionless grouping indicates when one subscale process dominates over the other

$$R_c = \frac{p_c^*}{aH\Delta\rho g}, \quad (1.6)$$

where a is the characteristic amplitude of the underlying roughness scaled by aquifer thickness H . When $R_c \gg 1$, the capillary fringe has a dominant impact on CO₂ migration, while roughness dominates when $R_c \ll 1$.

Together these dimensionless groupings allow us to evaluate the types of systems, as well as the appropriate length and timescales, for which the VE and gravity-capillary equilibrium assumptions are valid. Taking the first dimensionless grouping R_L , we find that many prospective storage sites for CO₂ sequestration have large aspect ratios. For instance in the Alberta Basin in Western Canada, each potential storage formation in the geological sequence is tens to a few hundred meters thick, while the areal extent of each layer is several hundred kilometers in each direction [1]. When considering the large spatial extent that must be modeled for industrial-scale CO₂ injection, on the order of 100 km² or more, then R_L^{-1} will be significantly less than unity.

When considering gravity segregation, we observe that typical CO₂-brine systems across a wide range of temperature and pressure regimes will have short timescale to segregation relative to the timescale of interest. For example, a cold-deep aquifer will have density contrast of 350–400 kg/m³, while at the other extreme, a warm-shallow aquifer will have a much larger contrast of up to 800 kg/m³ [3]. Another example is the Utsira formation [9], where a high permeability and strong density contrast lead to gravity segregation on the order of days, or $T_f \simeq 10^{-2}$ if we are interested in years of simulation.

The analysis of a capillary fringe is more difficult because often the capillary pressure curves are not known or are only estimated for a given storage formation. However, given some commonly used capillary pressure parameters from CO₂ modeling studies in the literature [13], the time to establish a capillary fringe will be anywhere from days to months. Therefore, the timescale of the simulation should be long relative to this in order to assume capillary-gravity equilibrium.

We may also consider whether a sharp interface is a good assumption, in which case the type of capillary pressure function assumed becomes important. If a typical Brooks–Corey type of function is used [8], then a fringe thickness of tens of meters can be expected. Therefore, if the formation thickness is on the same order of magnitude as the fringe, then the fringe must be modeled. For formations over 100 m thick, the fringe often can be reasonably replaced with a sharp interface. As we will discuss, the vertically integrated model can incorporate both cases in the model formulation, however the sharp-interface model is a simpler derivation and implementation.

3.2 Vertical fluid and pressure distribution

If pressure and gravity–capillary equilibrium are established within a short timescale relative to the simulation time, then the fluids are segregated and a well-defined vertical fluid structure exists in the aquifer. As a result, the vertical space can be subdivided into macroscopic regions bound by macroscopic interfaces, as depicted in Figure 1.4. The topmost region is created during the drainage process as CO₂ displaces brine. Region 1 contains mobile CO₂ and is bounded at the top by the ζ_T interface and at the bottom by a dynamic macroscale interface at a depth defined by $\zeta_M(x, y, t)$ that evolves in space and time. During the drainage process, ζ_M will move downward, but when flow reverses and brine reimbibes the pore space, residual CO₂ is trapped behind the receding ζ_M interface. This creates a residual CO₂ region that is bound above by the ζ_M interface and below by another dynamic interface $\zeta_R(x, y, t)$. The bottommost region of fluid is the undrained brine region bound above by ζ_R and below by the aquifer bottom at ζ_B .

The mobile CO₂ region may be subdivided into two regions if a capillary fringe exists and $\epsilon \gg 1$. We can define a top subregion that contains only mobile CO₂ and residual brine, which corresponds to fully drained conditions. The second sub-region consists of the capillary fringe where both CO₂ and brine are mobile with a transition in saturation from endpoint CO₂ saturation to endpoint brine saturation. The two sub-regions are separated by another dynamic interface $\zeta_F(x, y, t)$, where $\zeta_M \leq \zeta_F \leq \zeta_T$.

Due to this well-defined vertical structure, the following relation between the macroscopic interfaces must hold for the VE model,

$$\zeta_B \leq \zeta_R \leq \zeta_M \leq \zeta_F \leq \zeta_T. \quad (1.7)$$

When $\epsilon \ll 1$, the capillary fringe region disappears and $\zeta_F = \zeta_M$ everywhere.

At equilibrium, pressure and saturation distributions in the vertical dimension are defined according to density and capillarity. For instance, a fluid-statics calculation can be used to derive a vertical pressure profile for each phase given a general fluid density profile $\rho_\alpha(z)$ and a single pressure P_α at some datum level, $z = \zeta_P$,

$$p_\alpha(z) - P_\alpha = \mathbf{e}_z \cdot \mathbf{g} \int_{\zeta_P}^z \rho_\alpha(z') dz' \quad \alpha = c, b. \quad (1.8)$$

Here, we have chosen a coordinate system aligned with the large-scale aquifer dipping plane such that the \mathbf{e}_z is the coordinate perpendicular to the plane. Thus, the gravitational vector becomes $\mathbf{e}_z \cdot \mathbf{g} = -g \cos \theta$. For an incompressible system, equation (1.8) becomes

$$p_\alpha(z) = P_\alpha - \rho_\alpha g \cos \theta (z - \zeta_P), \quad (1.9)$$

which is depicted schematically in Figure 1.3. We note that there is no physical basis for defining the upscaled phase pressure at depths where the phase does not exist. However, in practice, the phase pressure can be extrapolated to the specified datum. Defining phase pressure in this way has no effect on the resulting model [53].

Given P_α as the upscaled phase pressure, we can define an upscaled capillary pressure

$$P_{\text{cap}}(x, y) = P_c(x, y) - P_b(x, y), \quad (1.10)$$

which can be related to the fine-scale capillary pressure p_{cap} as

$$p_{\text{cap}}[s_c(x, y, z)] = P_{\text{cap}}(x, y) + \Delta\rho g \cos \theta(z - \zeta_P). \quad (1.11)$$

Following [53], equation (1.11) can be used to reconstruct the fine-scale vertical saturation distribution $s_c(z)$,

$$s_c(z) = p_{\text{cap}}^{-1} [P_{\text{cap}} + \Delta\rho g \cos \theta(z - \zeta_P)]. \quad (1.12)$$

where p_{cap}^{-1} is the inverse of the fine-scale capillary pressure–saturation relationship. The $p_{\text{cap}}-s$ function is dependent on the formation rock and fluid properties and must be obtained through laboratory experiments on core samples. If the samples are tested under ambient conditions, they must be rescaled to reservoir conditions before being applied in this model.

Given a p_{cap} function, calculation of the inverse is generally done numerically. During primary drainage, the inverse of the primary drainage curve is straightforward. However, during imbibition, the local saturation at the time of reversal $s_c^*(z)$ will dictate the imbibition or scanning curve that must be inverted to reconstruct the saturation distribution. Local residual saturations $s_{cr}(z)$ are also dependent on the reversal saturation.

In general, the vertical structure of fluids for systems with large capillary transition zones, i.e. $\epsilon \gg 1$, are shown in Figure 1.3 and can be written mathematically as

$$s_c(z) = \begin{cases} 0, & \text{if } \zeta_B \leq z < \zeta_R \\ s_{cr}(s_c^*), & \text{if } \zeta_R \leq z < \zeta_M \\ p_{\text{cap}}^{-1}, & \text{if } \zeta_M \leq z < \zeta_F \\ 1 - s_{\text{br}}, & \text{if } \zeta_F \leq z \leq \zeta_T. \end{cases} \quad (1.13)$$

For the sharp-interface case ($\epsilon \ll 1$), the saturation distribution abruptly changes at the ζ_M interface with no transition zone (Figure 1.3). The mathematical description can then be greatly simplified as

$$s_c(z) = \begin{cases} 0, & \text{if } \zeta_B \leq z < \zeta_R \\ s_{cr}^0, & \text{if } \zeta_R \leq z < \zeta_M \\ 1 - s_{\text{br}}, & \text{if } \zeta_M \leq z \leq \zeta_T, \end{cases} \quad (1.14)$$

where s_{cr}^0 is the endpoint CO₂ residual saturation.

3.3 Model derivation

The model derivation presented here is restricted to immiscible and incompressible systems for convenience, but later we present the equations with compressibility and miscibility (CO_2 dissolution and convection). The top and bottom boundaries are modeled as impermeable in this derivation, however this is not a requirement and vertical flow through the caprock may be included if desired, such as through leaky abandoned wells [22].

To begin, we consider the three-dimensional mass conservation equations for CO_2 and brine phases at the fine-scale,

$$\frac{\partial}{\partial t} (\phi s_\alpha) + \nabla \cdot \mathbf{u}_\alpha = q_\alpha, \quad \alpha = c, b. \quad (1.15)$$

In the above equation, ϕ is porosity, s_α is the phase saturation, \mathbf{u}_α is the volumetric phase flux, and q_α is the volumetric source/sink term per unit volume. Here, \mathbf{u}_α is given by Darcy's law [5],

$$\mathbf{u}_\alpha = -\frac{k_\alpha \mathbf{k}}{\mu_\alpha} \cdot (\nabla p_\alpha - \rho_\alpha \mathbf{g}), \quad (1.16)$$

where \mathbf{k} is the permeability tensor, k_α is the phase relative permeability, μ_α is the phase viscosity, p_α is the phase pressure, ρ_α is the phase density, and \mathbf{g} is the gravitational vector. The fluids are immiscible such that dissolution of CO_2 into the brine-rich phase and vice versa is neglected.

The integration is performed between the bottom and top boundaries of the storage formation, assuming impermeable shale layers bound the system above and below. The vertical direction (z) is defined as perpendicular to the local dipping plane of the reservoir, such that flow is predominantly in the lateral direction (x and y). Due to the assumption of VE and gravity segregation, the CO_2 phase is bounded below by a dynamic macroscopic interface $\zeta_M(x, y, t)$, while the residual region of CO_2 created by imbibition is bounded by $\zeta_R(x, y, t)$. The resulting two-dimensional equations consist of integrated variables such as thickness of mobile and residual CO_2 regions and depth-integrated horizontal phase fluxes. The details of the integration can be found in previous work, see [22, 24, 28, 50], and will not be repeated in detail here. A brief overview of the integrated 2D equations is given.

After integration of equation (1.15), we obtain the upscaled lateral 2D mass conservation equations for components CO_2 and brine with upscaled variables (capital letters indicate vertically upscaled),

$$\frac{\partial}{\partial t} (H\Phi S_\alpha) + \nabla_{||} \cdot \mathbf{U}_{||\alpha} = Q_\alpha, \quad \alpha = c, b. \quad (1.17)$$

In the integrated equation, Φ is depth-averaged porosity, S_α is the depth-integrated saturation, $H(x, y)$ is spatially varying aquifer thickness, defined as $H(x, y) =$

$\zeta_T(x, y) - \zeta_B(x, y)$, Q_α is the depth-integrated source/sink term, and $(\cdot)_\parallel$ represents lateral operators and quantities. Depth-integrated saturation is defined as

$$H\Phi S_\alpha = \int_{\zeta_B}^{\zeta_T} \phi s_\alpha dz, \quad \alpha = c, b. \quad (1.18)$$

The volumetric fluxes $\mathbf{U}_{\parallel\alpha}$ are obtained by vertically integrating the lateral component of phase fluxes and gives the resulting upscaled flux expression

$$\mathbf{U}_{\parallel\alpha} = \int_{\zeta_B}^{\zeta_T} \mathbf{u}_{\parallel\alpha} dz, \quad \alpha = c, b. \quad (1.19)$$

After integration, assuming the lateral gradients in pressure $\nabla_\parallel p_\alpha$ are constant in the vertical dimension, the resulting depth-integrated flux expression is

$$\mathbf{U}_{\parallel\alpha} = -\frac{HK_{\parallel\alpha} \cdot \mathbf{K}_\parallel}{\mu_\alpha} \cdot (\nabla_\parallel p_\alpha - \rho_\alpha \mathbf{g}_\parallel), \quad \alpha = c, b. \quad (1.20)$$

where \mathbf{K}_\parallel is the depth-integrated permeability tensor given by

$$HK_\parallel = \int_{\zeta_B}^{\zeta_T} \mathbf{k}_\parallel dz, \quad (1.21)$$

and $\mathbf{K}_{\parallel\alpha}$ is the depth-integrated relative permeability tensor of phase α given by

$$HK_{\parallel\alpha} \cdot \mathbf{K}_\parallel = \int_{\zeta_B}^{\zeta_T} \mathbf{k}_\parallel k_\alpha dz, \quad \alpha = c, b. \quad (1.22)$$

For convenience, we will omit the $(\cdot)_\parallel$ notation from this point onward.

Based on the previous discussion regarding pressure equilibrium, we can replace the fine scale phase pressure with the expression for coarse scale pressure P_α from equation (1.9). For the expressions that follow $\zeta_P = \zeta_B$. Also, using the definition of coarse-scale capillary pressure from equation (1.11), we obtain expressions for local pressure distribution for each phase,

$$p_b = P + \mathbf{e}_z \cdot \mathbf{g} \rho_b (z - \zeta_B), \quad \text{for } \zeta_B \leq z \leq \zeta_M, \quad (1.23)$$

and

$$p_c = P + p^e + \mathbf{e}_z \cdot \mathbf{g} [\rho_b (\zeta_M - \zeta_B) + \rho_c (z - \zeta_M)], \quad \text{for } \zeta_M \leq z \leq \zeta_T, \quad (1.24)$$

with $P = P_b$ as the primary pressure variable and p^e as the capillary entry pressure at the CO₂-brine interface, i.e. $p^e = p_{\text{cap}}(\zeta_M)$. We see that the pressure is not obtained

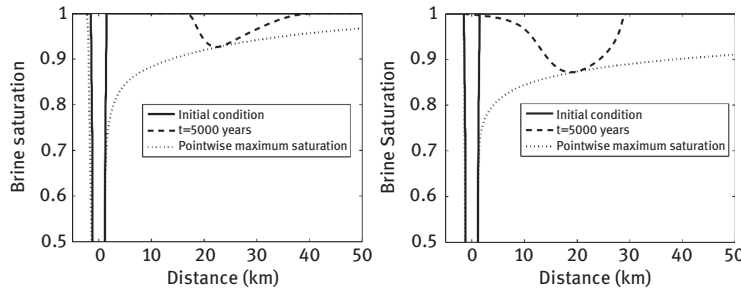


Figure 1.5: Influence of a capillary fringe and residual trapping on the plume extent after injection. The result of implementing the sharp interface model is shown left, while the resulting plume shape and extent from including both a capillary fringe and residual trapping is shown right. Figure adapted from Nordbotten and Dahle [53].

for a phase where it is immobile. By substitution of equations (1.23) and (1.24) into equation (1.20) we have

$$\mathbf{U}_b = -\frac{H\mathbf{K}_b \cdot \mathbf{K}}{\mu_b} \cdot [\nabla P - \nabla (\mathbf{e}_z \cdot \mathbf{g} \rho_b \zeta_B) - \rho_b \mathbf{g}], \quad (1.25)$$

and

$$\mathbf{U}_c = -\frac{H\mathbf{K}_c \cdot \mathbf{K}}{\mu_c} \cdot [\nabla P + \nabla p^e + \nabla (\mathbf{e}_z \cdot \mathbf{g} \Delta \rho \zeta_M) - \nabla (\mathbf{e}_z \cdot \mathbf{g} \rho_b \zeta_B) - \rho_c \mathbf{g}]. \quad (1.26)$$

Note that the z terms in equations (1.23) and (1.24) disappear when taking the lateral gradient of p_α . The spatial gradient of capillary entry pressure ∇p^e may also go to zero for homogeneous capillary properties.

Together, equations (1.17)–(1.26) represent the upscaled system of equations consisting of depth-integrated variables. The VE model, which can be solved analytically under certain simplifying assumptions, must be solved numerically for heterogeneous systems (see [25, 28]). The VE model must also resolve the topographical heterogeneity of the caprock to correctly capture fluid flow in a rough caprock system.

As previously discussed, the effect of a capillary fringe on plume migration has been studied by Nordbotten and Dahle [53], where an analytical solution of a physically reasonable scenario was also presented. Figure 1.5 shows a comparison of the sharp interface model with a model including both a capillary fringe and residual trapping. With the inclusion of a capillary fringe the plume shape is affected and the CO₂ does not reach the same lateral extent. The capillary fringe may thus have a marked influence on results when included in a VE model, where the fine scale dynamics within the fringe are upscaled and included in the upscaled capillary pressure function. Further complexities of the implementation of a capillary fringe include possible hysteretic behavior of the capillary pressure function and the residual trapping process.

3.4 Upscaling and subscale processes

The VE assumption and subsequent vertical integration is the foundation for the solution of lateral flow of multiple phases within a porous medium. Within this general framework, other important processes that affect CO₂ trapping and migration need to be included in the model formulation. These processes may or may not play a significant role in the long-term fate of CO₂ and greatly depends on subsurface conditions in the storage formation of interest and the length and timescales being considered. Often there is a mismatch between the scale of relevant processes and the scale of model resolution, and therefore some upscaling may be required. Here, we discuss the modeling aspects of compressibility, CO₂ dissolution with convection, and structural rugosity. Other subscale processes may be important, such as chemical and geomechanical processes, but these will not be discussed here.

3.4.1 Compressibility

Compressibility can impact CO₂ migration through both porosity and density changes that can vary as a function of fluid pressure. Density can also vary with temperature, but in the absence of leakage, this dependence is small in deep subsurface systems and can be neglected for simplicity. The impact of pressure is most relevant during injection, when pore pressures can increase by more than 10 MPa near the wellhead to drive CO₂ into the formation. As pressure increases, the storage capacity of a given volume of the formation increases due to expansion of the matrix and compression of the fluids. On the other hand, expansion of porosity can cause fracturing or large deformations that can be detected at the ground surface. Overpressurization can also induce seismicity and activate faults near the injection point.

Here we only consider linear elastic changes in porosity and small changes in fluid density but no phase transitions. For porosity, we define a matrix compressibility β_m which is a function of pressure:

$$\frac{d\phi}{dp} = \beta_m . \quad (1.27)$$

Similarly, fluid compressibility β_α is defined as

$$\frac{1}{\rho_\alpha} \frac{d\rho_\alpha}{dp_\alpha} = \beta_\alpha , \quad (1.28)$$

which can be integrated for constant β_α

$$\rho_\alpha = \rho_0 e^{\beta_\alpha (p_\alpha - p_0)} , \quad (1.29)$$

where ρ_0 is the known CO₂ density at some reference pressure p_0 .

VE models have been developed to include compressibility using different approaches. For instance, analytical VE models include slight compressibility in the

storage coefficient that allows for time dependence in the pressure solution [49, 50]. However, the fluid densities are constant in space and time and depend only on an average initial pressure and temperature in the storage formation [50]. A similar approach has been implemented numerically as well [23]. A recent correction has been developed that dynamically computes the average CO₂ density increase due to the pressure increase during injection. The density calculation iterates with the plume solution and pressure calculation, but the solution still assumes a constant density throughout the plume at each timestep.

More recent work has considered the vertical and horizontal change in CO₂ density within the VE framework [64]. CO₂ density increases with depth in a fluid-static system, and therefore the vertical pressure distribution at equilibrium [equation (1.8)] is a nonlinear function. We can approximate the dependence of CO₂ density on pressure by combining a Taylor expansion of equation (1.29) with the VE expression in equation (1.8) to get a linearized expression for static vertical profile for CO₂ pressure,

$$p_c(z) = P - G (1 + \beta_c(P_c - p_0)) (z - \zeta_B), \quad (1.30)$$

and for the CO₂ density vertical profile,

$$\rho_c(z) = a(h, P_c) + b(P_c)z, \quad (1.31)$$

where $G = \rho_0 g \cos \theta$ and

$$a = \rho_0 + \rho_0 \beta_c (P_c - p_0) + \rho_0 \beta_c G h_b + \rho_0 \beta_c^2 G (P_c - p_0) h_b, \quad (1.32)$$

$$b = -\rho_0 \beta_c G - \rho_0 \beta_c^2 G (P_c - p_0). \quad (1.33)$$

These more complicated vertical profiles are then used to formulate the VE model with compressible CO₂.

The VE model derivation with CO₂ compressibility (assuming incompressible brine and constant porosity) results in the following upscaled mass conservation equations,

$$\phi H \frac{\partial}{\partial t} (R_c S_c) + \nabla \cdot \mathbf{F}_c = 0. \quad (1.34)$$

In this equation, the upscaled density R_c is defined as

$$H R_c S_c = \int_{\zeta_B}^{\zeta_T} \rho_c s_c dz, \quad (1.35)$$

and the upscaled mass flux \mathbf{F}_c becomes

$$\mathbf{F}_c = \int_{\zeta_B}^{\zeta_T} \rho_c \mathbf{u}_c dz. \quad (1.36)$$

The integral expression results in a more complex definition of upscaled flux when substituting equations (1.30) and (1.31).

Assuming a sharp interface ($\epsilon \ll 1$), the CO₂ mass flux becomes

$$\begin{aligned} \mathbf{F}_c = & -\Lambda K R_c \nabla P + \Lambda_c K \beta_c G \nabla P \left[\frac{1}{2}a(H + h_b) + \frac{1}{3}b(H^2 + Hh_b + h_b^2) - hR_c \right] \\ & - \nabla h_b G(1 + \beta_c(P - p_0)) \Lambda_c K R_c + \Lambda_c K \hat{R}_c^2 g \sin \theta, \end{aligned} \quad (1.37)$$

where

$$R_c = a + \frac{1}{2}b(H + h_b), \quad (1.38)$$

$$\hat{R}_c^2 = a^2 + ab(H + h_b) + \frac{1}{3}b^2(H^2 + Hh + h^2), \quad (1.39)$$

and

$$\Lambda_c = \lambda_c^r \frac{H - h_b}{H}. \quad (1.40)$$

The brine equation leads to a similar expression to the incompressible case presented in Section 3.3, but with mass fluxes $\mathbf{F}_b = \rho_b \mathbf{U}_b$,

$$\Phi \rho_b \frac{\partial}{\partial t} (S_b) + \nabla \cdot \mathbf{F}_b = 0. \quad (1.41)$$

In real systems, the ability to handle compressibility of the matrix and brine is important for more accurate compositional and geomechanical effects. It is possible to extend the above derivation to a more general formulation, which is part of ongoing work in this area.

3.4.2 CO₂ dissolution with convective mixing

Another potentially important process is dissolution of CO₂ into the aqueous phase and subsequent transport of dissolved CO₂. Equilibrium partitioning can be assumed locally when both phases are present. In this case, local dissolution occurs instantaneously into the residual brine in the mobile CO₂ region ($\zeta_M \leq z \leq \zeta_T$) and into the mobile brine in the residual CO₂ region ($\zeta_R \leq z \leq \zeta_M$). Without convection, transport of dissolved CO₂ across the two interfaces into the pure brine region below is a diffusion-controlled process. However, if the potential for long-term convection will lead to acceleration of dissolution across these interfaces, then a more complex model is necessary. The unstable nature of the convective mixing process can be upscaled and incorporated as a subgrid mass transfer function, as was described in more detail in [24].

Convection can occur within the brine region ($\zeta_B \leq z \leq \zeta_R$) when a layer of CO₂-saturated brine is created at the ζ_R interface that is denser than “pure” brine below (brine with no dissolved CO₂). This system is inherently unstable, and the CO₂-saturated brine will sink toward the bottom of the aquifer and induce convective mixing

within the system. This system has been studied extensively by others [18, 20, 21, 39, 61, 65]. Although the fingering phenomenon is complex at the small scale, several aspects can be exploited in the simplified modeling framework. First, analytical and high-resolution analysis has shown that the onset time of instability is relatively short for typical systems, on the order of 1 year. This implies that the time dependence of the instability can be neglected if we are interested in timescales of hundreds of years. Furthermore, it has been shown that once the instability occurs, the effective total mass transfer rate is constant in time until the convective fingers interact with the bottom aquifer boundary. This effect allows for convective mixing to be easily upscaled as a constant rate parameter within the VE model.

To formulate the VE model with dissolution, an additional equation is needed to model the transport of dissolved CO₂ in the brine phase. In this model, mass transfer of CO₂ into the brine phase due to convective mixing is parameterized by ω , which is the average mass fraction of dissolved CO₂ in the region bounded by ζ_R and ζ_B . The onset of convective mixing is considered an instantaneous process and the up-scaled dissolution rate due to convective mixing is constant in time (but may vary in space due to heterogeneity). The transport equation is coupled with the horizontal flow equations that solve for pressure and saturation. When developing the model, it is necessary to formulate the flow equations more generally in terms of total mass of each component per unit area rather than depth-integrated saturations.

First, we define M^ι as the mass per area of component $\iota = c, b$ summed vertically over each fluid phase $\alpha = c, b$. The resulting component mass conservation equation becomes

$$\frac{\partial M^\iota}{\partial t} + \nabla_{||} \cdot \mathbf{F}^\iota = Q^\iota, \quad \iota = c, b, \quad (1.42)$$

where \mathbf{F}^ι is the total mass flux of component ι across all phases, and Q^ι is the source/sink term of component mass per area. The component mass flux equation is defined as

$$\mathbf{F}^\iota = \sum_{\alpha} \int_{\zeta_B}^{\zeta_T} \mathbf{u}_{\alpha} \rho_{\alpha} m_{\alpha}^\iota dz \quad \iota = c, b \quad \text{and} \quad \alpha = c, b, \quad (1.43)$$

where m_{α}^ι is the mass fraction of component ι in phase α at equilibrium as $m_{\alpha}^{\iota, eq}$.

The mass flux described above is composed of flow of a given component through the three main regions depicted in Figure 1.4. For example, if considering the flux of CO₂ across the aquifer, the CO₂-rich phase in the top region, (ζ_M, ζ_T), contains CO₂ at a mass fraction m_c^c , which depends on the solubility of water in CO₂. In the residual CO₂ region, (ζ_R, ζ_M), the brine phase contains dissolved CO₂ that is at equilibrium and only a function of CO₂ solubility at equilibrium m_b^c . And finally, the (ζ_B, ζ_R) region consists of fully saturated brine phase that contains dissolved CO₂ at some average mass fraction that is dynamic and a function of mass transfer across ζ_R driven by the convective process described in more detail below.

The mass-per-area of CO₂ dissolved in brine M_b^c is a conserved quantity that can be modeled with the following transport equation:

$$\frac{\partial M_b^c}{\partial t} + \nabla_{||} \cdot \int_{\zeta_B}^{\zeta_T} \mathbf{u}_b \rho_b m_b^c dz = C_{\text{diss}}(\omega, \zeta_R), \quad (1.44)$$

where the second term on the left-hand side represents the total flux of dissolved CO₂ in the brine phase, and the right-hand side represents the rate of CO₂ mass transfer into the brine phase due to dissolution across the ζ_R interface, which is influenced by convection. The rate parameter C_{diss} is the upscaled dissolution rate discussed above, with units of mass per area per time, which depends on ω , the normalized concentration of dissolved CO₂ in the brine region below the ζ_R interface, and the location of the ζ_R interface.

Due to the complexity of density-driven convection, the dynamics of the instability are not explicitly resolved but rather treated as a subgrid process. This means that all CO₂ that is dissolved below the ζ_R interface (as subscale convective fingers) is accounted for in the dimensionless concentration variable ω , which has a value between 0 and 1. Thus, the mass-per-area of dissolved CO₂ in the brine region is given as: $\omega h_{R,B} \rho_b^{\text{mix}} m_b^c$, where ρ_b^{mix} is the density of CO₂-saturated brine. The upscaled dissolution rate parameter C_{diss} is constrained by the value of ω and the location of the ζ_R interface. Under certain conditions, such as complete saturation of the brine column, C_{diss} may be zero, otherwise the value is the specified upscaled dissolution rate. When equation (1.44) is solved along with the flow equations, the evolution and transport of dissolved CO₂ is mass conservative and mathematically consistent.

The value of C_{diss} can be determined from numerical experiments or based upon dimensionless groupings. A number of detailed numerical and experimental studies have found that the overall mass transfer rate due to the dissolution-convection process is roughly constant in time after a finite onset time and before the convective fingers reach the bottom of the formation [57, 61, 65]. The rate of dissolution due to convective mixing is controlled by the Rayleigh number, and is most sensitive to permeability of the aquifer system and the value of the diffusion coefficient. Recent studies have shown that the rate may be parameterized by fluid and rock properties [46]. In addition, the impact of heterogeneity (i.e. horizontal layering) in the formation may substantially reduce the upscaled dissolution rate [17].

3.4.3 Rough caprock and rugosity

Caprock topography can play an important role in controlling the migration and trapping of CO₂ [28]. This phenomenon depends on structural variability, or roughness, of the caprock that can be characterized at different spatial scales ranging from kilometer- to centimeter-scale. The largest scale features, such as anticlines and other dome-like structures with associate spillpoints, can be easily detected in seismic

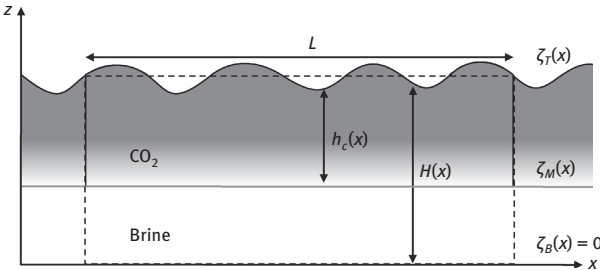


Figure 1.6: Caprock roughness at the horizontal fine-scale having spatially varying thickness $H(x)$ and CO_2 thickness $h_c(x)$ within the averaging length L . The system has a flat bottom $\zeta_B = 0$ and flat CO_2 -brine interface. Adapted from [27].

surveys [35] and have been shown to affect large-scale migration patterns such as the Sleipner injection [30]. However, the smallest variability, known as rugosity, exists below seismic detection limits ($\leq 10\text{ m}$) and can only be measured using LiDAR scans of formation outcrops [6, 36, 60]. Less is known about the actual impact of structural rugosity on CO_2 plume migration.

Neglecting caprock roughness, as is done in many simplified modeling studies [37, 42, 52], can lead to overestimation of plume migration speeds over 100-year timescales [28]. These models also neglect the impact of roughness on structural trapping, which could contribute significantly to a long-term storage security. Given the potential impact of subscale caprock roughness, it is necessary to model CO_2 migration without relying on traditional and expensive grid refinement techniques. Caprock roughness that exists below the scale of the model resolution must be handled by upscaling. To do this, the VE equations presented in Section 3.3 are integrated horizontally to obtain effective permeability and relative permeability functions that reflect the subscale variability, thus allowing the rough caprock to be replaced by a flat surface over the averaging scale. Large-scale caprock topography above the model resolution scale can still be resolved in the usual way.

The rough caprock upscaling approach is based on steady-state flow-based homogenization techniques that have been traditionally used to upscale permeability and relative permeability of heterogeneous media. In the case of effective permeability, the heterogeneity at the horizontal fine-scale is in caprock structure rather than permeability. Similarly, the heterogeneity in relative permeability is due to variability in CO_2 thickness under a rough caprock rather than heterogeneity in small-scale saturation. These effective functions can be derived for sharp-interface or capillary fringe-dominated systems.

Analytical effective functions for permeability, \bar{K} , and relative permeability, \bar{K}_α , can be derived for a vertical cross-section (x - z) of an aquifer (Figure 1.6). Horizontally upscaled variables are indicated with an overbar. For simplicity, this system has a flat bottom $\zeta_B(x) = 0$, and gravity is neglected. The objective of upscaling is to

replace the varying top boundary with a flat surface over the averaging volume. This results in an aquifer height that is constant and equal to the average of the thickness at the horizontal fine-scale over the averaging length,

$$\bar{H} = \frac{1}{L} \int_0^L [\zeta_T(x) - \zeta_B(x)] dx . \quad (1.45)$$

The basic approach is to posit a homogeneous equation at the average scale composed of horizontally averaged quantities. If we assume steady-state flow over the averaging length then the fine-scale single-phase flow equation can be integrated and set equal to the homogeneous equation

$$F_x = \frac{1}{L} \int_0^L \left(-\frac{HK}{\mu} \frac{dP}{dx} \right) dx = -\frac{\bar{H}\bar{K}}{\mu} \frac{\Delta P}{\Delta L} , \quad (1.46)$$

from which we obtain

$$\frac{1}{\bar{H}\bar{K}} = \frac{1}{L} \int_0^L \frac{1}{HK} dx . \quad (1.47)$$

Equation (1.47) indicates that the effective transmissibility ($\bar{H}\bar{K}$) for an aquifer of varying thickness is the harmonic average of fine-scale transmissibility over the length scale of interest.

For effective relative permeability \bar{K}_α , additional assumptions are required regarding the saturation at the horizontal fine-scale. Our approach is based on the capillary equilibrium assumption [47, 58] that is adapted to the VE rough caprock system and becomes an assumption on the CO₂–brine interface. For small pressure gradients and a horizontal averaging length much smaller than the domain, the ζ_M interface is essentially flat. This means that $\nabla\zeta_M = 0$ in equations (1.25) and (1.26), and the fine-scale saturations can be fixed during the averaging step. Then in a similar manner shown in equation (1.46), the two-phase steady-state flow equation is compared with the corresponding homogeneous equation, which results in upscaled relative permeability of the form

$$\frac{1}{\bar{H}\bar{K}\bar{K}_\alpha} = \frac{1}{L} \int_0^L \frac{1}{h_\alpha K K_\alpha} dx . \quad (1.48)$$

We observe that the effective relative permeability is a harmonic mean of fine-scale relative permeability values weighted by the corresponding transmissibility. For CO₂, this implies that if $h_c(x) = 0$ at any point within the averaging window then $\bar{K}_c = 0$. Therefore, CO₂ has zero mobility for locations of the CO₂ interface equal to or higher than the local minimum of the topography.

Numerical homogenization can be performed by simulating steady-state flow at the fine-scale with the nonupscaled VE model. The average flux can be calculated and

used to determine the effective permeability and relative permeability from the homogeneous equations. For 2D caprock surfaces, numerical homogenization is almost always necessary.

4 Model application

The utility of a simplified model can be demonstrated by application to realistic CO₂ storage systems. We present a comparison of the simplified VE model with a fully three-dimensional simulator for CO₂ migration within a structurally heterogeneous system. Then, we show VE model results for different systems where small-scale processes such as capillarity, dissolution and caprock roughness are important factors for CO₂ migration and trapping. These model results show that upscaling can be an effective means for modeling important physical processes without expensive grid refinement or complex model coupling. This capability is especially important for large scale systems of tens of kilometers in lateral dimension, where full-physics simulators are not able to feasibly resolve the submeter scale phenomena in long-term simulations. In these cases, the VE model is the only practical simulation tool.

Several benchmark studies have shown that the VE model compares well with full three-dimensional simulators [10, 28, 55], which is an indication of the effectiveness and reliability of the simplified approach. In these benchmarks, the three-dimensional results are often assumed to be the standard or true model result against which the simplified model is measured, however, in certain cases, the VE model can produce a more reliable solution. This is true especially in gravity-dominated systems with sharp changes in caprock topography. In Figure 1.7, three such results are given using the ECLIPSE simulator, each with increasing vertical resolution. The last figure in this series gives the result of the same problem after simulation using a VE model. The ECLIPSE simulations can be seen to converge to the VE result with increasing resolution, which is to be expected since upscaling can be seen as implementing a model with infinite vertical resolution. Thus, as long as the VE assumption is practically valid, a VE model should provide the most accurate solution with the least computational expense.

Given successful benchmarking of the VE model against other simulators, some recent work has focused on comparison to real-field data. The top layer of the Utsira formation, known as Layer 9, has been monitored by seismic surveys since injection began in 1996 [9]. The seismic data indicate a gravity-dominated system that has led to fast segregation of CO₂ and brine, with CO₂ migrating by buoyancy along the complex topography at the top of the Utsira. The basic VE model presented in Section 3 has been applied to this system, which assumes an incompressible, immiscible system and a sharp interface between the CO₂ and resident brine. In Figure 1.8 a comparison is made between seismic data of CO₂ in the top layer of the Utsira formation observed in 2006 [9] with the result of a simulation using a VE model. There is qual-

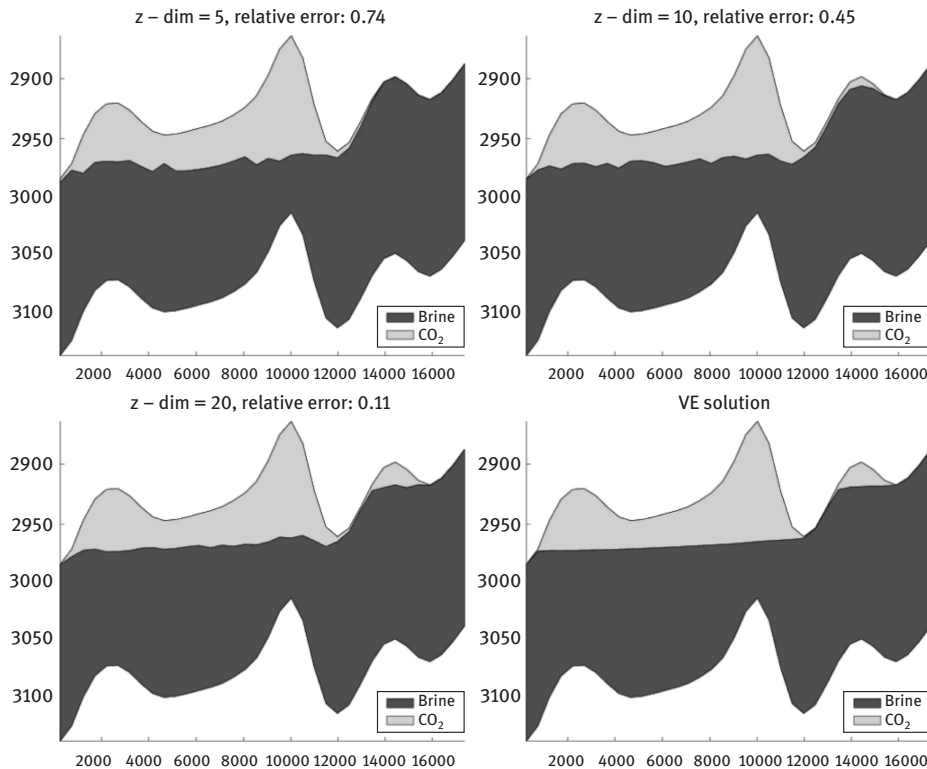


Figure 1.7: Comparison of full two-phase, three-dimensional ECLIPSE simulations, showing the CO₂ distribution after 2000 years, with increasing vertical resolution (leftmost figures), with a VE simulation [69].

itative agreement of the CO₂ plume shape between the seismic representation and the VE simulation result. This provides confidence for expanding the basic VE model to have the capability to model more complicated processes and to study their effects, if any, on the CO₂ migration.

Given the high permeability of the unconsolidated sand in the Utsira formation, it is likely that convection has been initiated in Layer 9 due to the dissolution of CO₂ into brine across the large-scale interface, ζ_M . Gravimetric data taken along the sea floor suggests that total dissolution rates from the CO₂ plume could be as high as 1.8% of the injected mass per year [2], providing some evidence of convective mixing in the Utsira formation. A recent study has used this field-scale data to determine the magnitude of the upscaled convection-enhanced dissolution rate C_{diss} used in the extended VE model discussed in Section 3.4. The total rate of dissolution from the plume is sensitive to both the value of C_{diss} and the areal footprint of the plume, which itself depends on various system parameters such as permeability, porosity and CO₂

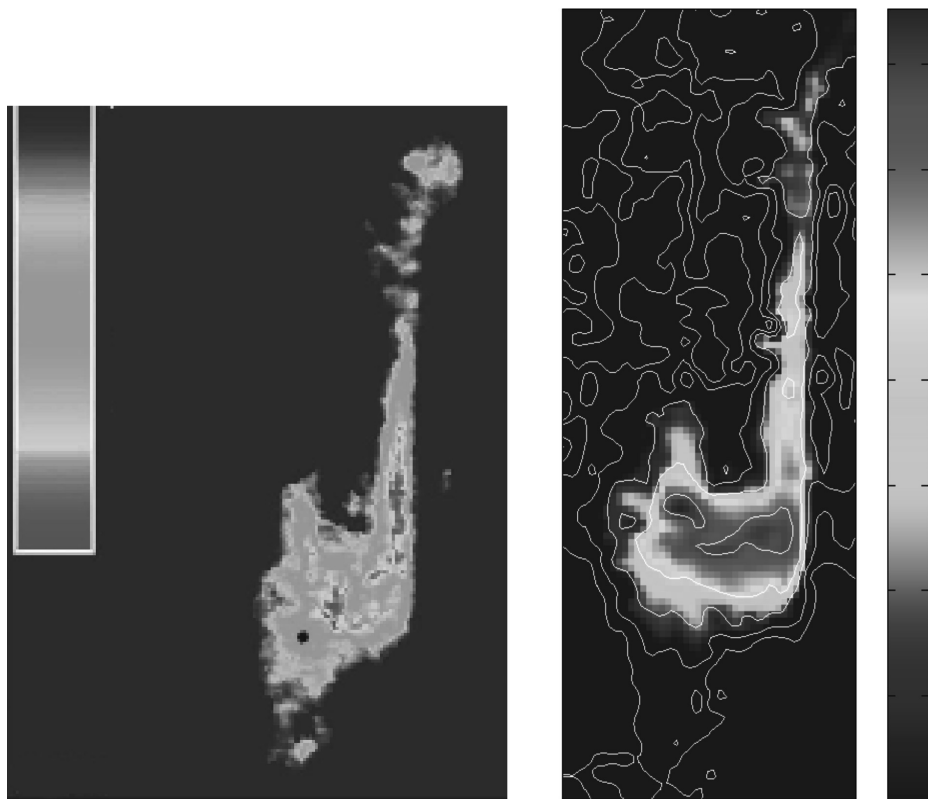
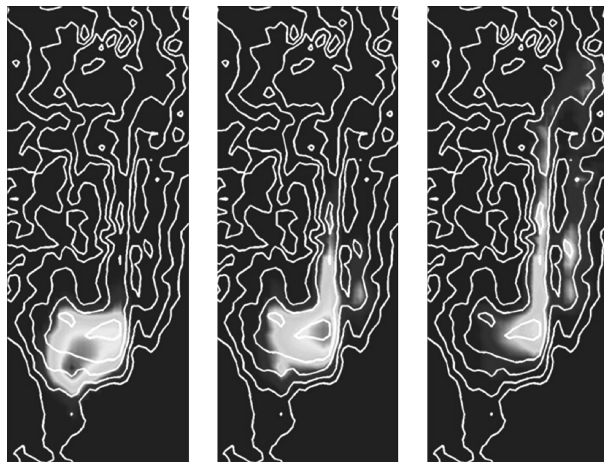


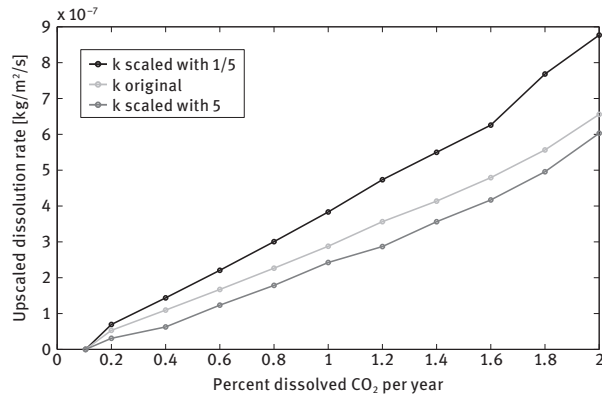
Figure 1.8: Comparison of seismic data (adapted from [9]) for CO₂ accumulation in Layer 9 of the Utsira formation in 2006 (left) with history matching via a VE simulation with a sharp-interface assumption and no dissolution (right). Results were obtained using the MRST code (available at <http://www.sintef.no/Projectweb/MRST/Gallery/CO2-storage/>). Color scale for the seismic data is the scaled amplitude of the seismic signal. Color scale for simulation data is CO₂ thickness ($\in [0, 1]$) scaled by formation thickness of Layer 9.

density. Figure 1.9 compares increasing values of permeability in this chapter on dissolution rates and shows the resulting plume spread after seven years of injection into Layer 9. Although a direct comparison to the data shown in Figure 1.8 was not the objective of this chapter, it is clear that increasing permeability provides a better match to the seismic data. More importantly, by matching to the 1.8% upper bound given by the gravimetric study, this chapter shows that upscaled dissolution rates could be as high as 30 kg/m²/year. From these results it is clear that convective mixing could provide significant dissolution potential at the field scale, thus increasing the long-term storage security of CO₂ in the Utsira formation and similar North Sea operations.

We emphasize that the unstable process of convective mixing at very small scales combined with the large-scale gravity- and topography-dominated nature of CO₂ mi-



(a) Simulated CO₂ plume with different permeability scalings – 1/5 (left), 1 (middle), and 5 (right).



(b) C_{diss}

Figure 1.9: Plume migration (a) and upscaled dissolution rate (b) for CO₂ injection in the topmost layer of the Sleipner field with increasing scalings of the original permeability from 1/5 to 5. Results are shown after 7 years of injection into Layer 9 and correspond to 2006 data. Estimates of dissolution rate determined using the VE model with convective mixing. Figure adapted from Mykkeltvedt and Nordbotten [45].

gration is difficult if not impossible to model with a fully three-dimensional model using traditional grid refinement techniques. If a fully 3D simulator contains an up-scaled representation of the convective mixing process, then enhanced dissolution can be described correctly, although no such upscaling has been demonstrated to date. In any case, the VE model is an important and practical tool for estimating field-scale dissolution rates for CO₂ storage systems and understanding sensitivity of

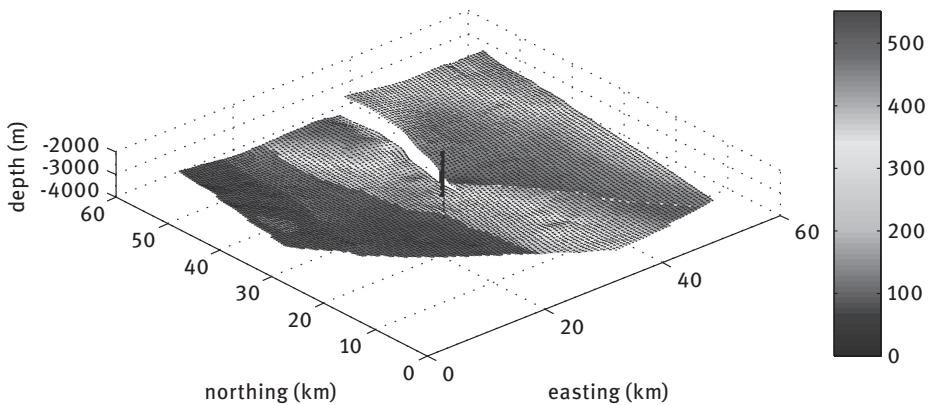


Figure 1.10: The full-field Johansen formation (sector 5 dataset) courtesy of SINTEF. Shown are aquifer geometry, permeability distribution (mDarcy), and location of the injection well. Adapted from [25].

the system to uncertainty in the parameter space. The utility of the VE model is further demonstrated by simulations of CO₂ injection into the Johansen formation, another prospective site for CO₂ storage in the North Sea [25]. The full-field Johansen formation is a large-scale heterogeneous system, 60 km in lateral dimension (Figure 1.10), and injection is anticipated to be 4 million tons annually, four times larger than currently injected into the Utsira formation [15].

The VE model was applied to the hypothetical Johansen injection given the permeability and porosity data and a reasonable estimate of constitutive functions such as capillary pressure and relative permeability [15]. As opposed to the Utsira example above, there is no data against which to measure the impact of a capillary fringe or convection-enhanced dissolution on CO₂ migration and trapping in the Johansen formation. Therefore, the parameter space was explored in a series of VE simulations, i.e. sharp interface compared to capillary fringe, and upscaled convection-dissolution rate of 1 kg/m²/year versus no convective effects. An example of VE model results for all relevant physics is given in Figure 1.11, which show the plume migrating 10 km from the injection site, following the dip and large-scale topography of the formation. Dissolved CO₂ sinks below the plume and residual CO₂ is trapped behind the receding front. The relative amount of trapped CO₂ is highly dependent on which processes are modeled (Figure 1.12). These results demonstrate the importance of reliable data for capillary pressure and convective mixing processes for understanding the fate of CO₂ over 1000-year timescales.

The final application of the VE model relates to the impact of subscale caprock roughness on CO₂ migration. Realistic caprock roughness data is not currently available, but the impact of topography and ability of the horizontally upscaled model discussed in Section 3.4 can be explored for an idealized aquifer cross-section [26, 27].

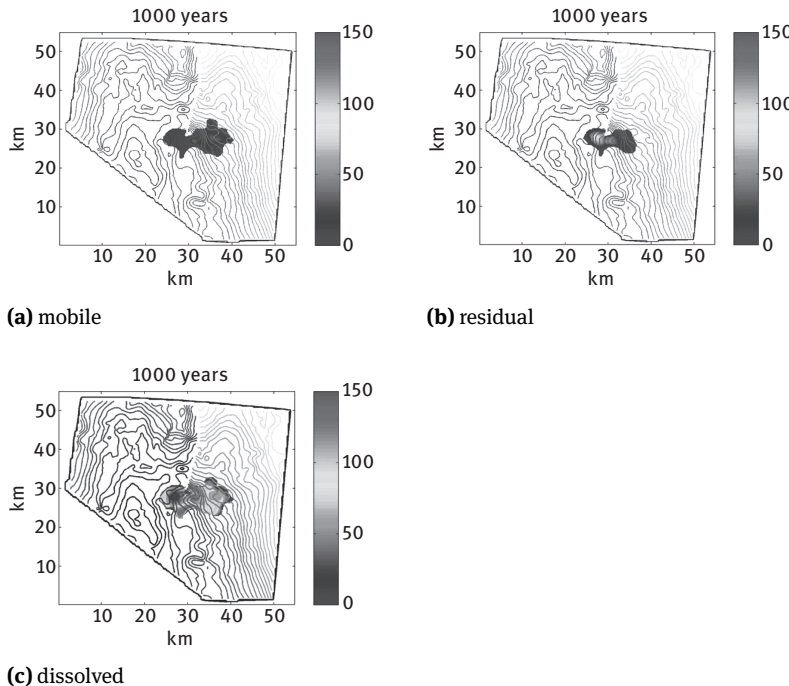


Figure 1.11: VE model results of postinjection CO₂ migration for the case with all relevant processes—capillary fringe, convection-enhanced dissolution, and residual trapping. Shown is the thickness in meters of (a) mobile CO₂, (b) residual CO₂, and (c) dissolved CO₂ at 50, 500, and 1000 years. Adapted from [25].

Simulations of CO₂ migration were performed in a system with a top surface $\zeta_T(x)$ described by a sinusoidal function,

$$\zeta_T(x) = \bar{H} (1 + \alpha \sin \omega x), \quad \zeta_B(x) = 0, \quad (1.49)$$

with scaled amplitude $\alpha = A/\bar{H} = 0.1$, wavelength $\omega = 0.01\pi$, and average aquifer thickness $\bar{H} = 100$ m. Given a sharp interface, we can apply equations (1.47) and (1.48) to compute the effective permeability and analytically for this system,

$$\bar{K} = k\sqrt{(1 - \alpha^2)}, \quad \bar{K}_c = k_c^r \frac{\sqrt{(\bar{h}_c/\bar{H})^2 - \alpha^2}}{\sqrt{1 - \alpha^2}}, \quad \bar{K}_b = \frac{\bar{h}_b}{\bar{H}}. \quad (1.50)$$

The resulting CO₂ relative permeability curve (Figure 1.13) has zero mobility until CO₂ fills the traps. Once CO₂ is mobile, the relative permeability is reduced due to the impact of caprock roughness on the migration speed of thin CO₂ plumes. For the case including a capillary fringe, the integration can be performed numerically, and the resulting functions reflect both the impact of a capillary fringe (convexity) and the topography (reduced mobility at low CO₂ saturations) on upscaled CO₂ relative permeability.

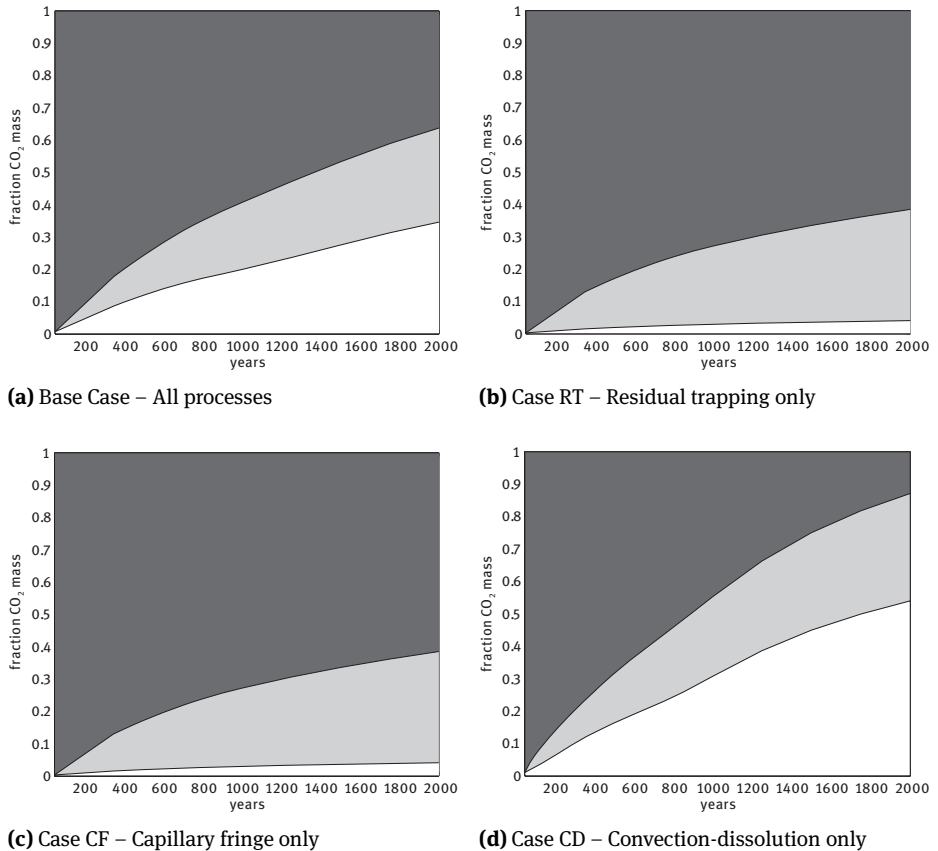
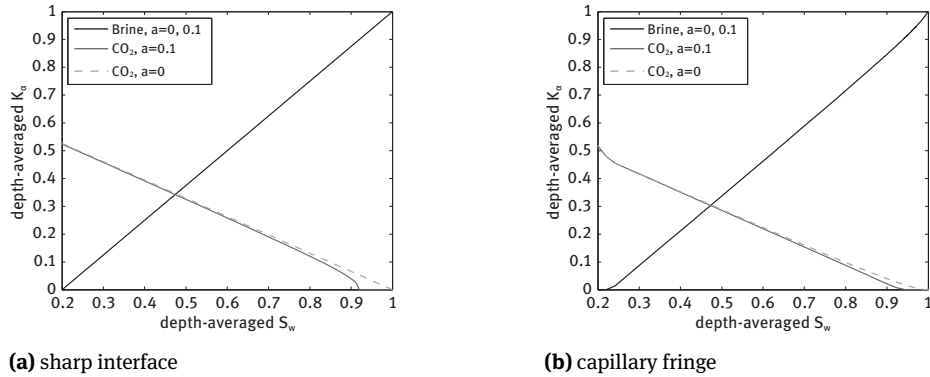


Figure 1.12: Distribution of CO₂ mass for the base case with all relevant processes modeled (a) compared with different model cases where only one process is modeled at a time (b)–(d). Mobile CO₂ is the dark region, residually trapped CO₂ is the medium gray region, and dissolved CO₂ is the light gray region. Adapted from [25].

The resulting migration is impacted by topography when compared with a flat smooth caprock (Figure 1.14). In both the sharp interface and capillary fringe cases, the plume reaches only a fraction of the distance after 1000 years of migration when roughness slows the migration speed (Figure 1.15). The capillary fringe with caprock roughness results in the slowest migration speed. The capillary fringe impacts CO₂ migration through the convexity of the upscaled relative permeability curves, leading to a reduction of CO₂ migration that is equivalent to the impact of caprock roughness. This behavior of the plume is expected in this case, since the dimensionless grouping $R_c \approx 1$ (Section 3.1).

The effective model compares well in this 1D case with the resolved simulations in both the sharp-interface and capillary fringe cases. The horizontally upscaled model

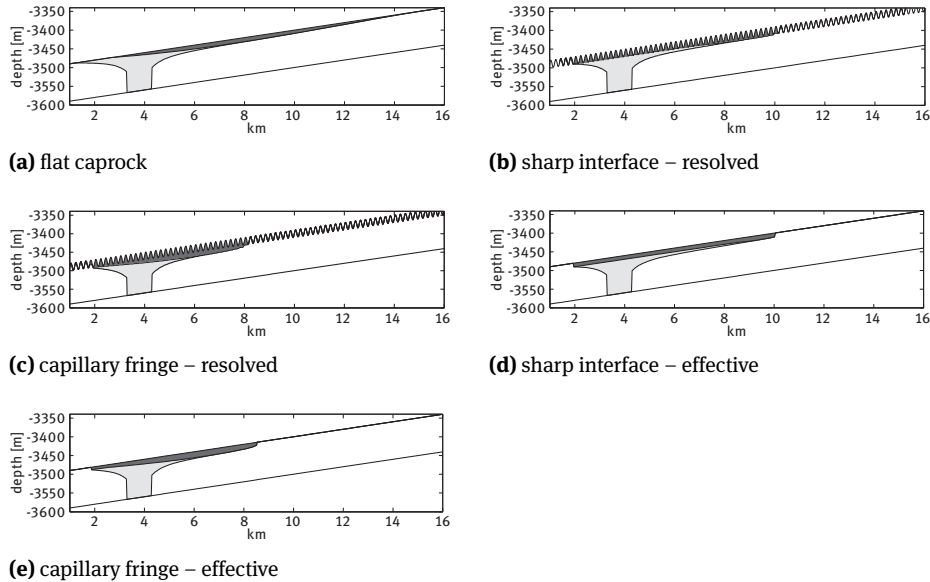


(a) sharp interface

(b) capillary fringe

Figure 1.13: Upscaled relative permeability functions for a caprock surface

$\zeta_T(x) = \bar{H}(1 + \alpha \sin x)$ assuming a sharp interface (a) and a capillary fringe (b). CO₂ curves are shown for $\alpha = 0.1$ and $\alpha = 0$. Adapted from [26].

**Figure 1.14:** Resolved and effective model results for CO₂ plume (dark) and residual trapping (light) for an idealized rough caprock (b)–(e) compared with a flat smooth caprock (a). Adapted from [26].

can also be extended to caprock surfaces to understand the impact of roughness on CO₂ migration in both lateral dimensions [27]. We conclude from this work that effective constitutive functions can be easily derived if caprock roughness parameters such as the dominant amplitude and shape of the structures can be obtained from

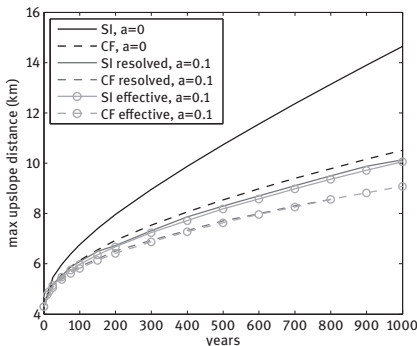


Figure 1.15: Maximum upslope extent of CO₂ over time for resolved and sharp interface and capillary fringe effective simulations. Adapted from [26].

geological and geophysical characterization of the formation. Thus, we can greatly simplify the geological model and reduce the need for expensive grid refinement. More efficient simulation of complex CO₂ systems allows for exploring uncertainty and assessing long-term migration of CO₂ in realistic systems.

5 Summary

Modeling of injection and long-term behavior of supercritical CO₂ into underground repositories is an enormously challenging task due to large spatial and temporal scales and the importance of complex physical processes occurring on relatively short scales.

In this chapter, we have reviewed upscaling based on VE methods as an alternative to standard simulation tools to perform fast and relatively accurate simulations. This type of modeling can efficiently be used in history matching and to create risk scenarios. Benchmarking has shown that these methods in many cases give as accurate and even better results than standard full 3D-simulations. These methods are also currently able to account for many of the most important processes relevant for CO₂ sequestration.

We summarize some of the findings regarding the state-of-the-art in VE methods and their potential for future application:

- Several dimensionless groupings can be used to analyze the range of validity of the VE assumption in terms of spatial/temporal scales and geological parameters. The assumption of VE is typically relevant in the postinjection period when vertical segregation is achieved. However, simulation studies based on data from the Utsira injection show that these methods also could be useful in the injection period for modeling the spreading of the plume in the top layer of the formation in gravity-dominated systems.

- The sharp interface approximation is the simplest variant of the VE methods and greatly simplifies calculations. This approximation applies to systems where the capillary transition zone is small relative to aquifer thickness. The result is a CO₂ plume that spreads quickly and leads to large migration distances. It also gives upper estimates on time before immobilization of the plume.
- Capillary effects can easily be included to account for residual saturations and a capillary fringe. Accurate estimates of residual saturations are important in order to have good estimates of time to plume immobilization. The capillary fringe reduces the advance of the plume. Work is in progress to include more realistic hysteresis models for capillary effects.
- In large-scale simulations dissolution can only be modeled by estimates for effective mass transfer rates. Such models have been included in VE simulations of realistic CO₂ injection sites. However, the main focus is still to understand the convection process at the fine scale, in particular in the presence of formation heterogeneity. Accurate estimates of dissolution rates are very important for quantifying time to immobilization.
- Compressibility of porosity and CO₂ density due to increasing pore pressure during injection can be modeled in the VE framework. The model implementation is currently in progress, and therefore the importance of CO₂ compressibility has not been demonstrated. We expect that since CO₂ is much more compressible than brine, it may be necessary to accurately model large changes in density during injection rather than assuming a constant density as is usually done in simplified models. Reservoir conditions near the critical point may also require a more accurate compressibility model.
- Recently, the impact on CO₂ migration due to variations in caprock topography has been included into the VE formulation. Subscale traps in the caprock may significantly affect migration speed and immobilization of the plume. In modeling the impact of topography, we must consider the resolution of structural features at the geological scale versus the computational scale to determine whether upscaling is necessary. Additionally, the strength of the structural impact will depend on the vertical dimension of the topography compared to thickness of the plume defined by the gravity override and the capillary fringe.
- Geochemistry has up to now not been included in these models. It is possible that geochemical reactions can be handled in a similar manner as dissolution. However, we hypothesize that effects of fluid-rock reactions can only be modeled by some accuracy if the fine-scale fluid distribution can accurately be reconstructed along the vertical axis.
- Some progress has been shown in terms of the coupling between fluid flow and geomechanics. However, this may be the most important/outstanding topic for further research.
- The development of simplified models such as VE models is critical for understanding all relevant processes that impact CO₂ migration and trapping over large

spatial and temporal scales. Under the appropriate conditions, the VE model can be more efficient and accurate than a full 3D-simulator that must resolve small-scale phenomena. More efficient models are well-suited for exploring the parameter space, an essential aspect of assessing and mitigating the risks associated with long-term geological CO₂ storage operations.

References

- [1] Alberta Geological Survey, *Geological Maps*. <http://www.agi.gov.ab.ca>, 2011.
- [2] H. Alnes, O. Eiken, S. Nooner, G. Sasagawa, T. Stenvold, and M. Zumberge, Results from Sleipner gravity monitoring: Updated density and temperature distribution of the CO₂ plume, *Energy Procedia* 4 (2011), 5504–5511.
- [3] S. Bachu, Sequestration of CO₂ in geological media: Criteria and approach for site selection in response to climate change, *Energy Conversion Management* 41 (2000), 953–970.
- [4] S. Bachu, Screening and ranking of sedimentary basins for sequestration of CO₂ in geological media in response to climate change., *Environmental Geology* 44 (2003), 277–289.
- [5] J. Bear, *Dynamics of Fluids in Porous Media*, American Elsevier Publication Co., New York, NY, 1972.
- [6] J. A. Bellian, C. Kerans, and D. C. Jennette, Digital outcrop models: Applications of terrestrial scanning lidar technology in stratigraphic modeling, *Journal of Sedimentary Research* 75 (2005), 166–176.
- [7] M. J. Bickle, Geological carbon storage, *Nature Geoscience* 2 (2009), 815–818.
- [8] R. H. Brooks, and A. T. Corey, Properties of Porous Media Affecting Fluid Flow, *Journal of the Irrigation and Drainage Division, Proceedings of the American Society of Civil Engineers* IR2 (1966), 61–88.
- [9] R. A. Chadwick, P. Zweigle, U. Gregersen, G. A. Kirby, S. Holloway, and P. N. Johannessen, Geological reservoir characterization of a CO₂ storage site: The Utsira Sand, Sleipner, Northern North Sea, *Energy* 29 (2004), 1371–1381.
- [10] H. Class, A. Ebigo, R. Helmig, H. K. Dahle, J. M. Nordbotten, M. A. Celia, P. Audigane, M. Daracis, J. Ennis-King, Y. Q. Fan, B. Flemisch, S. E. Gasda, M. Jin, S. Krug, D. Labregere, A. N. Beni, R. J. Pawar, A. Sbai, S. G. Thomas, L. Trenty, and L. L. Wei, A benchmark study on problems related to CO₂ storage in geologic formations, *Computational Geosciences* 13 (2009), 409–434.
- [11] K. H. Coats, R. L. Nielsen, M. H. Terune, and A. G. Weber, Simulation of three-dimensional, two-phase flow in oil and gas reservoirs, *SPE Journal* Dec (1967), 377–388.
- [12] K. H. Coats, J. R. Dempsey, and J. H. Henderson, Use of vertical equilibrium in 2-dimensional simulation of 3-dimensional reservoir performance, *SPE Journal* 11 (1971), 63–71.
- [13] B. Court, K. W. Bandilla, M. A. Celia, J. M. Nordbotten, M. Dobossy, and A. Janzen, Applicability of vertical-equilibrium and sharp-interface assumptions in carbon sequestration modeling, *International Journal of Greenhouse Gas Control* 10 (2012), 134–147.
- [14] D. L. Dietz, A theoretical approach to the problem of encroaching and by-passing edge water, in: *Proceedings of Akademie van Wetenschappen*, 56-B, p. 83, 1953.
- [15] G. T. Eigestad, H. K. Dahle, B. Hellevang, F. Riis, W. T. Johansen, and E. Øian, Geological modeling and simulation of CO₂ injection in the Johansen formation, *Computational Geosciences* 13 (2009), 435–450.
- [16] M. T. Elenius, *Convective Mixing in Geological Carbon Storage*, Ph.D. thesis, University of Bergen, Norway, 2011.

- [17] M. T. Elenius and S. E. Gasda, Impact of tight horizontal layers on dissolution trapping in geological carbon storage, in: *Proceedings of XIX International Conference on Computational Methods in Water Resources*, 17–22 June 2012, University of Illinois at Urbana-Champaign, Urbana, IL, USA, 2012.
- [18] M. T. Elenius, J. M. Nordbotten, and H. Kalisch, Effects of a capillary transition zone on the stability of a diffuse boundary layer, *IMA Journal of Applied Mathematics* 77 (2012), 771–787.
- [19] R. M. Enick and S. M. Klara, CO₂ solubility in water and brine under reservoir conditions, *Chemical Engineering Communications* 90 (1990), 23–33.
- [20] J. Ennis-King and L. Paterson, Role of convective mixing in the long-term storage of carbon dioxide in deep saline formations, *SPE Journal* 10 (2005), 349–356.
- [21] R. Farajzadeh, H. Salimi, L. J. P. Zitha, and H. Bruining, Numerical simulation of density-driven natural convection in porous media with application for CO₂ injection projects, *International Journal of Heat and Mass Transfer* 50 (2007), 5054–5064.
- [22] S. E. Gasda, J. M. Nordbotten, and M. A. Celia, Vertical equilibrium with sub-scale analytical methods for geological CO₂ sequestration, *Computational Geosciences* 13 (2009), 469–481.
- [23] S. E. Gasda, J. M. Nordbotten, and M. A. Celia, Vertical equilibrium with sub-scale analytical methods for geological CO₂ sequestration, *Computational Geosciences* 13 (2009), 435–450.
- [24] S. E. Gasda, J. M. Nordbotten, and M. A. Celia, Vertically-averaged approaches for CO₂ injection with solubility trapping, *Water Resources Research* 47 (2011), W05528.
- [25] S. E. Gasda, J. M. Nordbotten, and M. A. Celia, Application of simplified models to CO₂ migration and immobilization in large-scale geological systems, *International Journal of Greenhouse Gas Control* 9 (2012), 72–84.
- [26] S. E. Gasda, H. Nilsen, and H. Dahle, Effective models for CO₂ migration in geological systems with varying topography, in: *Proceedings of XIX International Conference on Computational Methods in Water Resources*, 17–22 June 2012, University of Illinois at Urbana-Champaign, USA, 2012.
- [27] S. E. Gasda, H. Nilsen, H. Dahle, and W. G. Gray, Effective models for CO₂ migration in geological systems with varying topography, *Water Resources Research* 48 (2012), W10546.
- [28] W. G. Gray, P. Herrera, S. E. Gasda, and H. K. Dahle, Derivation of vertical equilibrium models for CO₂ migration from pore scale equations, *International Journal of Numerical Analysis and Modeling* 9 (2012), 745–776.
- [29] W. G. Gray, A. Leijnse, R. L. Kolar, and C. A. Blain, *Mathematical Tools for Changing Spatial Scales in the Analysis of Physical Systems*, CRC Press, Boca Raton, FL, 1993.
- [30] C. Hermanrud, T. Andresen, O. Eiken, H. Hansen, A. Janbu, J. Lippard, H. N. Bolås, T. H. Simmenes, G. M. G. Teige, and S. Østmo, Storage of CO₂ in saline aquifers-Lessons learned from 10 years of injection into the Utsira Formation in the Sleipner area, *Energy Procedia* 1 (2009), 1997–2004.
- [31] M. A. Hesse, F. M. Orr, and H. A. Tchelepi, Gravity currents with residual trapping, *Journal of Fluid Mechanics* 611 (2008), 35–60.
- [32] M. A. Hesse, H. A. Tchelepi, B. J. Cantwell, and F. M. Orr, Gravity currents in horizontal porous layers: Transition from early to late self-similarity, *Journal of Fluid Mechanics* 577 (2007), 363–383.
- [33] H. E. Huppert and A. W. Woods, Gravity-driven flows in porous layers, *Journal of Fluid Mechanics* 292 (1995), 55–69.
- [34] L. Ingeborg, and H. M. Nilsen, Numerical aspects of using vertical equilibrium models for simulating CO₂ sequestration, in: *Proceedings of 12th European Conference on the Mathematics of Oil Recovery: ECMOR XII*, 6–9 September 2010, Oxford, UK, 2010.

- [35] C. A.-L. Jackson, H. Grunhagen, J. A. Howell, A. L. Larsen, A. Andersson, F. Boen, and A. Groth, 3D seismic imaging of lower delta-plain beach ridges: Lower Brent Group, northern North Sea, *Journal of the Geological Society* 167 (2010), 1225–1236.
- [36] R. R. Jones, K. J. W. McCaffrey, P. Clegg, R. W. Wilson, N. S. Holliman, R. E. Holdsworth, J. Imber, and S. Waggett, Integration of regional to outcrop digital data: 3D visualisation of multi-scale geological models, *Computers and Geosciences* 35 (2009), 4–18.
- [37] R. Juanes, C. W. MacMinn, and M. L. Szulczewski, The footprint of the CO₂ plume during carbon dioxide storage in saline aquifers: Storage efficiency for capillary trapping at the basin scale, *Transport in Porous Media* 82 (2010), 19–30.
- [38] L. W. Lake, *Enhanced Oil Recovery*, Prentice-Hall, Englewood Cliffs, NJ, 1989.
- [39] E. Lindeberg, P. Bergmo, and A. Moen, The long-term fate of CO₂ injected into an aquifer, in: *Proceedings of the 6th International Conference on Greenhouse Gas Control Technologies* (J. Gale and Y. Kaya, eds.), Pergamon, Kyoto, Japan, 2003.
- [40] E. Lindeberg, and D. Wessel-Berg, Vertical convection in an aquifer column under a gas cap of CO₂, *Energy Conversion Management* 38 (1997), S229–S234.
- [41] C. Lu, S.-Y. Lee, W. S. Han, B. J. McPherson, and P. C. Lichtner, Comments on “abrupt-interface solution for carbon dioxide injection into porous media” by M. Dentz and D. Tartakovsky, *Transport in Porous Media* 79 (2009), 29–37.
- [42] C. W. MacMinn, and R. Juanes, Post-injection spreading and trapping of CO₂ in saline aquifers: Impact of the plume shape at the end of injection, *Computational Geosciences* 13 (2009), 483–491.
- [43] J. C. Martin, Partial integration of equations of multiphase flow, *SPE Journal* 8 (1968), 370–380.
- [44] B. Metz, *IPCC Special Report on Carbon Dioxide Capture and Storage*, Cambridge University Press, Cambridge, 2005.
- [45] T. S. Mykkeltvedt, and J. M. Nordbotten, Estimating effective rates of convective mixing from commercial-scale injection, *Environmental Earth Sciences* (2012), 1–9, doi: 10.1007/s12665-012-1674-3.
- [46] J. A. Neufeld, M. A. Hesse, A. Riaz, M. A. Hallworth, H. A. Tchelepi, and H. E. Huppert, Convective dissolution of carbon dioxide in saline aquifers, *Geophysical Research Letters* 37 (2010), L22404.
- [47] I. Neuweiler, and H.-J. Vogel, Upscaling for unsaturated flow for non-Gaussian heterogeneous porous media, *Water Resources Research* 43 (2007), W03443.
- [48] H. Nilsen, P. Herrera, M. Iding, C. Hermanrud, J. Nordbotten, K. A. Lie, and H. Dahle, Field-case simulation of CO₂-plume migration using vertical-equilibrium models., in: *Proceedings of 10th International Conference on Greenhouse Gas Control Technologies*, Amsterdam, The Netherlands., 2010.
- [49] J. M. Nordbotten and M. A. Celia, Similarity solutions for fluid injection into confined aquifers, *Journal of Fluid Mechanics* 561 (2006), 307–327.
- [50] J. M. Nordbotten and M. A. Celia, *Geological Storage of CO₂: Modeling Approaches for Large-Scale Simulation*, John Wiley & Sons, Inc., Hoboken, NJ, 2012.
- [51] J. M. Nordbotten, M. A. Celia, S. Bachu, and H. K. Dahle., Semi-analytical solution for CO₂ leakage through an abandoned well, *Environmental Science and Technology* 39 (2005), 602–611.
- [52] J. M. Nordbotten, M. A. Celia, D. Kavetski, and S. Bachu, A semi-analytical model estimating leakage associated with CO₂ storage in large-scale multi-layered geological systems with multiple leaky wells, *Environmental Science and Technology* 43 (2009), 743–749.
- [53] J. M. Nordbotten and H. K. Dahle, Impact of the capillary fringe in vertically integrated models for CO₂ storage, *Water Resources Research* 47 (2011), W02537.

- [54] J. M. Nordbotten, D. Kavetski, M. A. Celia, and S. Bachu, Model for CO₂ leakage including multiple geological layers and multiple leaky wells, *Environmental Science and Technology* 43 (2009), 743–749.
- [55] J. M. Nordbotten, B. Flemisch, S. E. Gasda, H. M. Nilsen, Y. Fan, G. E. Pickup, B. Wiese, M. A. Celia, H. K. Dahle, G. T. Eigestad, and K. Pruess, Uncertainties in practical simulation of CO₂ storage, *International Journal of Greenhouse Gas Control* 9 (2012), 234–242.
- [56] S. Pacala and R. Socolow, Stabilization wedges: Solving the climate problem for the next 50 years with current technologies, *Science* 305 (2004), 968–972.
- [57] G. S. H. Pau, J. B. Bell, K. Pruess, A. S. Almgren, M. J. Lijewski, and K. N. Zhang, High-resolution simulation and characterization of density-driven flow in CO₂ storage in saline aquifers, *Advances in Water Resources* 33 (2010), 443–455.
- [58] G. E. Pickup and K. D. Stephen, An assessment of steady-state scale-up for small-scale geological models, *Petroleum Geoscience* 6 (2000), 203–210.
- [59] M. Preisig and J. H. Prévost, Coupled multiphase thermo-poromechanical effects. Case study: CO₂ injection at In Salah, Algeria, *International Journal of Greenhouse Gas Control* 4 (2011), 225–230.
- [60] J. K. Pringle, R. L. Brunt, D. M. Hodgson, and S. S. Flint, Capturing stratigraphic and sedimentological complexity from submarine channel complex outcrops to digital 3D models, Karoo Basin, South Africa, *Petroleum Geoscience* 16 (2010), 307–330.
- [61] K. Pruess, *Numerical Modeling Studies of The Dissolution-Diffusion-Convection Process During CO₂ Storage in Saline Aquifers*, Lawrence Berkeley National Laboratory, Report no. LBNL-1243E, 2008.
- [62] K. Pruess and N. Muller, Formation dry-out from CO₂ injection into saline aquifers: 1. Effects of solids precipitation and their mitigation, *Water Resources Research* 45 (2009), W03402.
- [63] K. Pruess, T. F. Xu, J. Apps, and J. Garcia, Numerical modeling of aquifer disposal of CO₂, *SPE Journal* 8 (2003), 49–60.
- [64] S. R. Reistad, *Impact of compressibility in vertically integrated models for CO₂ storage*, Master's thesis, University of Bergen, Norway, 2012.
- [65] A. Riaz, M. Hesse, H. A. Tchelepi, and F. M. Orr, Onset of convection in a gravitationally unstable diffusive boundary layer in porous media, *Journal of Fluid Mechanics* 548 (2006), 87–111.
- [66] J. Rutqvist, D. W. Donald, and L. Meyer, Coupled reservoir-geomechanical analysis of CO₂ injection and ground deformations at In Salah, Algeria, *International Journal of Greenhouse Gas Control* 4 (2010), SI 225–230.
- [67] Schlumberger Information Systems, *ECLIPSE technical description*, Report, Houston, TX, 2007.
- [68] G. Schnaar and D. C. Digiulio, Computational modeling of the geologic sequestration of carbon dioxide, *Vadose Zone Journal* 2 (2009), 389–403.
- [69] MatMoRA webpage, <http://www.sintef.no/Projectweb/MatMorA/>, 2011.
- [70] Y. C. Yortsos, A theoretical analysis of vertical flow equilibrium, *Transport in Porous Media* 18 (1995), 107–129.

